

## Review #1

The manuscript by Goldberg et al. is a valuable and timely analysis of NO<sub>x</sub> emissions during KORUS-AQ. It identifies some potential issues with NO<sub>x</sub> emissions in the region that are useful for air quality management as well as other works studying pollution during this campaign period. The work also has relevance beyond KORUS-AQ in terms of how OMI data is used to estimate NO<sub>x</sub> from urban areas, and also how TROPOMI data will be used in such studies in the future. The article is in general quite clear and easy to read, and most figures are useful and essential.

That being said, the work misses a critical opportunity to evaluate one of their main hypotheses, which is that regionally-derived NO<sub>2</sub> columns (using air mass factors from high-resolution WRF-Chem simulations) lead to objectively better NO<sub>x</sub> inversions. In fact, while they report the difference between these NO<sub>x</sub> inversions and those based on the standard OMI NO<sub>2</sub> data, the differences aren't critically evaluated, which is a shame, as it seems to be a rather easy next step. This would thus be my primary suggestion for revision. A few other aspects such as how using AMFs derived from a model that is clearly inaccurate to begin with affect their analysis, why spatial averaging is presented and then discarded, and why the regionally-derived NO<sub>2</sub> columns may be overestimating NO<sub>2</sub> in rural areas need to also be addressed.

Details of these comments as well as other are presented below; addressing them likely constitutes major revisions as additional WRF-Chem calculations are required.

Thank you for your comments; they have substantially improved our manuscript.

### Major comments:

✓Section 3.6: It isn't clear to me why the authors test a doubling of the emissions. The prior bottom-up values are 198, the top-down using standard product are 353 (an increase of x1.78) and the top-down using the regional product are 484 (an increase of x2.44). The test increase of x2 thus does little to distinguish between these two. This is a bit of a disappointment, as a major conclusion from this work is that the regional product (and top-down emissions using this product) are significantly different and better than the standard product. However, the only evidence presented that the regional product is better than standard thus far is the comparison to Pandora data. While encouraging, the authors are missing an big opportunity to make this argument much stronger by performing two model simulations for the entire KORUS-AQ period with top-down emissions that match those derived using the standard product and the regional product, precisely, and not some estimate of x2 that is neither here nor there. These two different model simulations can then be evaluated using the aircraft data.

In this revised manuscript, we have completed a month-long simulation with NO<sub>x</sub> emissions increased by a factor of 2.13, and have removed the two-day 2 × NO<sub>x</sub> scenario. A factor of 2.13 is chosen because the top-down estimate from the satellite is 484 kton/yr, while the top-down approach applied to the model is 227 kton/yr. The bottom-up NO<sub>x</sub> emissions inventory within a 40 km radius of Seoul is 198 kton/yr, however the 227 kton/yr value is a more appropriate comparison with the top-down satellite analysis.

We are confident the OMI-Regional NO<sub>2</sub> product is more robust than the standard product due to the comparison with the Pandora NO<sub>2</sub> network. Furthermore, the methodology of updating the satellite

product with high-resolution a priori NO<sub>2</sub> shape profiles is more scientifically appropriate for regional studies (Russell et al., 2012, Lamsal et al., 2015, Kuhlmann et al., 2016, Goldberg et. al., 2017).

Thus, we feel that it is unnecessary to perform a simulation with NO<sub>x</sub> increased by a factor of 1.56 (353 kton/yr vs. 227 kton/yr). Furthermore, as we show in two new figures, the updated 2.13 x NO<sub>x</sub> simulation agrees well with the aircraft data (Figure 9) and the OMI-Regional NO<sub>2</sub> product (Figure 10).

**√**General: Model values of NO<sub>2</sub> column are much lower than regionally-derived OMI NO<sub>2</sub> column in most areas, including rural areas (Fig 3). However model values match the aircraft data in rural areas (i.e. the only major discrepancies noted in discussion of Fig 5 or e.g. the conclusions (12.17-19)). What are we thus to make then of the quality of the regionally-derived OMI values in rural areas? Too high? This should be discussed. If these are too high, will the background values estimated in the EMG value thus be too high, and this error propagate into an error in the urban emissions?

In the original figure, we are referring to the “mainland transect”. This is a subset of the rural areas, and was inappropriate. We have since updated the figure to include all mainland areas away from Seoul, and now find a discrepancy between NO<sub>2</sub> in the lowest layers between the model and the aircraft observations. This figure and corresponding discussion has been updated.

**√**General: If model columns are too low, how does that impact model calculated AMF? How much would AMF change if using posterior emissions in WRF-Chem? An additional calculation of AMFs based on WRF-Chem simulations with adjusted emissions needs to be performed to answer this question.

A new figure, Figure 11, now addresses this. The effect of the emissions inventory on the air mass factor is appreciable, but is secondary to the resolution of the model simulation. In the Seoul metropolitan area, the AMF changes on average by 35% when switching from GMI to WRF-Chem and changes by only 8% when switching emission inventories.

**√**Or perhaps the NO<sub>2</sub> profiles in WRFChem are adjusted to account for this bias (this is indicated on 4.23, but no details are provided as to what this adjustment is, or how it is derived)? I try to evaluate the WRF-Chem profiles visually, based on Fig 5, but this plot doesn’t make that information clearly visible given the way the vertical axis isn’t strictly used (i.e. model and aircraft data collected at the same height are not plotted at the same height – which I understand from the perspective of clarity in showing their differences with box-whisker plots, but something else is needed to evaluate profile shapes).

The OMI-Regional NO<sub>2</sub> product derived herein already accounts for any mean model biases. A better description of this process is now provided in Section 2.1.1.

**√**General: if results with spatial ave kernel are not trusted for analysis, they should be removed throughout from the results. Otherwise, it is a bit of a distracting / potentially misleading presentation. For example on page 12, line 5 – this isn’t used, so why is it highlighted here? Still, wouldn’t there be some data from KORUS-AQ with which wind field estimates in WRF could be evaluated? It just seems a bit subjective here that this source of error is singled out (11.18) as justification for not using this approach, whereas profile shapes that come from WRF-Chem are deemed acceptable, even though WRF-Chem NO<sub>2</sub> column values are significantly biased low in urban areas. Further, it seems that

comparison to the Pandora data in Fig 6 would indicate that the spatial kernel adjustment is improving, rather than degrading, the column estimates, which is a point in favor of this approach.

As noted, the spatial averaging kernel provides important insight into resolving discrepancies between OMI NO<sub>2</sub> and Pandora NO<sub>2</sub>. However, we also emphasize that the spatial averaging kernel has its limitations. The top-down approach is extremely sensitive to wind direction, so any errors in the forecasted wind fields will propagate through to the top-down method. When we apply a spatial averaging kernel to the satellite retrieval and then perform the top-down method, a NO<sub>x</sub> emissions rate cannot be derived. Therefore, for the top-down analysis, the artificial error introduced by spatial averaging kernel outweighs its benefits. However, for the Pandora comparison, the benefits outweigh the artificial errors (as shown in Figure 6).

✓9.30-34: Not sure how this statement about NO<sub>x</sub> diurnal variability contributes to the difference between modeled and observed NO<sub>2</sub> columns. Are the authors suggesting that the diurnal variability of NO<sub>x</sub> emissions in Korea is incorrect? Simply noting that it is different than modeled diurnal variability in the US is not sufficient evidence and in fact comes across as tangential, unless the authors are claiming that NO<sub>x</sub> source profiles (EGUs, distribution of diesel vehicles in the transportation fleet) are identical, which seems dubious. So I suggest removing Fig 4, unless this argument can be substantially strengthened.

We are suggesting that the temporalization of NO<sub>x</sub> emissions can introduce errors in satellite and aircraft measurements, which occur during the daytime. The temporalization is a best estimate based on literature, but it is almost certainly not correct either. The temporalization of NO<sub>x</sub> emissions as a major source of the discrepancy has not been discussed in previous literature and is quite critical to the conclusions of this manuscript. Resolving these differences is an important topic for future research.

However, we are not necessarily suggesting that the Korean temporalization is identical to the eastern US, but instead are providing a comparison to show how temporalization can differ by region.

The discussion of this topic in the text has been added to and is now referenced in the Conclusions as an important source of the discrepancy.

✓Additionally, I wonder to what extent excessive NO<sub>2</sub> deposition in the model might be contributing to the noted differences; this could be driven by e.g. PBL heights in the model that are too low. I suspect there is more information from the KORUS-AQ campaign that could be used to evaluate this.

We have now included a comparison with NO<sub>y</sub>. Evaluating the NO<sub>2</sub> deposition rates and PBL heights is beyond the scope of this study.

✓Fig 5 and associated text: I agree this suggests the differences between WRF-Chem and OMI near Seoul are likely driven by emissions, rather than chemistry, deposition, or PBL heights, as suggested by the authors or myself.

✓10.20: Thoughts on why bias improves but not correlation? This might suggest that the daily variability of WRF-Chem (which impacts daily AMFs) is not correct, or at least not an improvement upon larger-scale averages.

Yes, these are our thoughts too. The WRF simulation used to drive the chemistry is in forecast mode. This has been clarified in the text.

✓General: How does the plume analysis / rotation / EMG inversion process work if e.g. there is a large point source whose outflowing plume flows over another source (e.g. a highway) that runs parallel underneath it, replenishing NO<sub>2</sub> concentrations that are then going to be ascribed only to emissions at a single point of plume origin? So, related, at 11.10: Yes, but the concern is rather smaller sources within this radius but not at the center that contribute to the plume (i.e. mobile sources).

Small sources at the edge of the urban boundary will lead to an artificially longer NO<sub>2</sub> lifetime. This partially compensates the error introduced by the wind. A short commentary has now been included in the Section 3.6.2 of the manuscript.

Minor comments and corrections:

✓Throughout: “shape profiles” reads a bit strange. Change to “profile shapes”? Or just profiles?

Updated

✓1.25: for the → for 1.26: “larger near large” rewrite

Updated

✓2.4-5: “another . . . another” rewrite

Updated

✓3.27: trace-gas Eq. 2: include a proper summation index

Updated

✓4.5-6: It isn’t clear here if the authors are discussing how AMFs are calculated in general, in the standard retrieval, or in their own regionally-specific retrieval. Please clarify.

It is in reference to all OMI NO<sub>2</sub> products derived from the NASA OMI NO<sub>2</sub> product. This includes both the standard product and the regional product derived here (as well as any other custom products derived from the NASA product). It has been clarified.

✓5.1: How big of an assumption is this, that the profiles are constant over this time range?

Please reference Laughner et al., 2016, which is already cited here. That study shows that the AMF can vary by 20% on a daily basis.

✓6.26: I’m pretty sure AOD from geostationary satellites over Korea have been used for forecasting studies.

The sentence referring to this simulation as the first near real-time application of geostationary data has been removed.

√6.26: Not sure though how the authors here qualify their study as “nearreal time”; all I saw was reanalysis. NRT usually means forecasting. Just because the winds were forecast within the domain doesn’t mean this is a chemical forecast, since the observations used span the time period over which the analysis (aircraft obs) are made (considerably, given that satellite data for several more years and months are used). This entire approach would be impossible in an NRT setting, given the data requirements for oversampling.

This statement is in reference to the model simulation only. The model simulation was indeed performed as a forecast in near-real time. The OMI NO<sub>2</sub> satellite data was processed after the fact, but AOD was in fact assimilated in near-real time.

√7.28: plume, → plume

Updated

√8.6: Why using wind estimates from a different model than the one used to constrain WRF met at the boundary (NCEP), or different from WRF itself?

The WRF simulation is a forecast simulation. Re-analysis data is more robust despite it being at a coarser spatial resolution.

√8.8: Why 500m? Based on Fig 5 it looks like NO<sub>2</sub> plumes extend much higher than that, up to 1 km or possibly above (although a bit hard to tell from this plot, given the manner in which the vertical scale is treated).

We follow Lu et al., 2015. Generally, winds do not vary much between 500 – 1000 m. De Foy et al., 2014 discuss how the selection of wind speeds/direction affect the top-down calculation. This is taken into account in the uncertainty analysis.

√Fig 1: content → concentration

The word “content” is correct in this context. Concentration is mass per unit volume, which is not being shown here.

√Fig 1: Why showing US domain?

This has now been removed, but the US is still referenced in the text for comparison.

√9.4: is in despite of --> is despite

Updated

√Section 3.1: Inclusion of / comparison to the US feels tangential and unnecessary. Suggest focus on Korea domain; remove US from Fig 1 and remove discussion here. This point could be touched on in intro or conclusions but doesn’t fit well in the results.

The US figure has now been removed, but the US is still quickly referenced in the text of this section for comparison.

✓9.17: There are also small decreases in the southern part of the peninsula, as well the SE corner of the domain. Further, the explanation provided for the decreases isn't particularly insightful.

This sentence has been removed.

✓9.21: From the presence of red in panel (c), the statement "in all areas" does not seem to accurately describe the results. Please update text to more precisely reflect the findings.

The word "all" has been changed to "most"

✓Section 3.3.1: it's not good style to have only one subsub section in a section. Consider merging this with 3.3 or making 3.3 WRF-Chem evaluation, 3.3.1 comparison to OMI and 3.3.2 comparison to aircraft.

This section is now a section by itself, since it is now expanded.

## Review #2

In “A top-down assessment using OMI NO<sub>2</sub> suggests an underestimate in the NO<sub>x</sub> emissions inventory in Seoul, South Korea during KORUS-AQ,” the authors combine two lines of research by 1) adjusting space-based retrievals of tropospheric NO<sub>2</sub> columns with spatially refined model data and then 2) estimating NO<sub>x</sub> emissions, NO<sub>x</sub> lifetime and background tropospheric NO<sub>x</sub> by applying an Exponentially Modified Gaussian fit to the resulting NO<sub>2</sub> column field. The authors test their method using model results that had been generated for forecasting purposes (which they determine to be successful by comparing top-down estimate to a bottom-up integration of emissions within what seems to be an arbitrary 40 km radius of Seoul).

√In general, the paper is well-written and is relevant to Atmospheric Chemistry and Physics.

Thank you for your comments; they have substantially improved our manuscript.

√I have two major concerns. The authors ignore impacts of topography and local circulations on the spatial gradients of the NO<sub>2</sub> column, the quantity that determines NO<sub>2</sub> lifetime and emissions in the analysis. Seoul is in a mountain basin terrain at the coast with further impacts on local atmospheric circulations from urban land use (e.g., <https://www.atmos-chem-phys.net/13/2177/2013/acp-13-2177-2013.pdf>).

We agree that it is important to reference the complex topography and meteorology of the area as sources of uncertainty, but we do not expect this source of uncertainty to bias our results in any particular direction. We have added a paragraph in the discussion section and now reference the aforementioned study and others.

The complex geography of the region further supports the use of our 4 x 4 km<sup>2</sup> simulation because it will capture topography and mesoscale phenomena better than a coarse global model.

When re-processing the air mass factor we use surface pressure of the WRF-Chem simulation to process the air mass factor, so we are already accounting for topographical differences in surface pressures. This is already discussed in Section 2.1.1.

√Also, the use of KORUS data in this manuscript for understanding the problem is limited, or is non-existent as it relates to understanding the NO<sub>2</sub> lifetime and NO<sub>y</sub> partitioning. The authors can use this opportunity to analyze the KORUS-AQ dataset, to compare observed NO<sub>x</sub>/NO<sub>y</sub> partitioning versus the NO<sub>2</sub> lifetime inferred in their analysis. The authors state that the NO<sub>2</sub> lifetime is not necessarily related to the true chemical lifetime (P12, L22-23), but the theoretical framework for the EMG method assumes that is the case, as NO<sub>x</sub> lifetime, emissions and background concentration are the only variables affecting total integrated NO<sub>2</sub> mass.

We have now included a comparison to NO<sub>y</sub> from the DC-8 aircraft. This is now shown in Figures 5 & 9. The large underestimate of NO<sub>y</sub> further supports the conclusions of our manuscript and makes it stronger.

It is beyond the scope of this study to do a full analysis of the NO<sub>y</sub> partitioning.

√I also recommend that the authors evaluate more than two days of model-observation comparisons in the assessment of the updated CTM simulation and add to the discussion (Fig. 9, P11 L29 – P12 L2) .

As suggested, a CTM simulation with  $2.13 \times \text{NO}_x$  for the entire month of May 2016 is now included.

This paper and the KORUS dataset provides an excellent opportunity to address the above complications and concern and I recommend the authors add more detailed analysis and discussion before publication.

Additional comments:

√P1: L21-22: “regional NASA OMI NO<sub>2</sub> product” clarify wording as this is not an official NASA product but rather is regional inputs to a NASA tropospheric SCD product

Updated

√L25-26: Do the reported scalar quantities refer to integrated mass or a scalar difference at a single point?

The scalar quantity for Seoul is within a 40 km radius. This has been clarified in Section 3.2, which is the section this statement is referencing.

√L30-32: Consider clarifying

√P2: L3: “Ideal” – this is strange wording as some ozone production occurs nearly everywhere in the troposphere with sufficient light at wavelengths less than 405 nm. Net production is another question.

Re-phrased to say, “In the presence of abundant volatile organic compounds and strong sunlight, NO<sub>x</sub> can participate in a series of chemical reactions to accelerate the production of O<sub>3</sub>”.

√L6-7: Consider word choice. Lightning is also a source. Furthermore, there is a large difference between budget and burden, which seems to be confused here. For example, the largest contributor to the atmospheric burden of NO<sub>2</sub> is stratospheric N<sub>2</sub>O photolysis.

Re-phrased to say, “There are some biogenic emissions of NO<sub>x</sub> (e.g., lightning), but the majority of the NO<sub>x</sub> emissions are from anthropogenic sources”.

√L8: I recommend changing the wording “NO<sub>2</sub> is one of the easiest trace gases to observe” to commenting that there is a rich legacy of NO<sub>2</sub> measurements by remote sensing that has been validated.

This paragraph has been re-worded as suggested.

√P3: L4: Consider inclusion of Zhou et al. Zhou, Y., D. Brunner, R. J. D. Spurr, K. F. Boersma, M. Sneep, C. Popp and B. Buchmann, Accounting for surface reflectance anisotropy in satellite retrievals of tropospheric NO<sub>2</sub>. Atmos. Meas. Tech., 3, 1185-1203, 2010. Zhou, Y., D. Brunner, K. F. Boersma, R. Dirksen, and P. Wang, An improved tropospheric NO<sub>2</sub> retrieval for OMI observations in the vicinity of mountainous terrain. Atmos. Meas. Tech., 2, 401-416, 2009.

## Included

**VP4:** L23-24: Please explain in more detail how “vertical profiles are scaled based on a comparison with in situ aircraft observations”

An extra sentence has been added: “For example, if the aircraft observations show that NO<sub>2</sub> concentrations between 0 - 500 m are low by 50%, then we scale the modeled NO<sub>2</sub> in this altitude bin by this same amount.”

As shown now shown in Figure 11, this has a minimal effect on the calculation of vertical tropospheric column contents over the Korean peninsula.

**VP5:** L1: “We used May 2016 monthly mean values” Please briefly mention here whether data outside of May 2016 will be used in the top-down emissions

Yes, these data are also included in the top-down analysis. A sentence has been added: “In the top-down emissions derivation, we use all nine-months of OMI data for the analysis.”

**VP6:** L26-27: I am quite skeptical that this is the first time that geostationary products have been used in a forecasting framework. E.g., <https://journals.ametsoc.org/doi/abs/10.1175/2008WAF2222165.1>

This sentence has been removed.

**VL31:** Does “enhancements” mean additions to the inventory or does it mean modifications to the inventory? Please clarify

The main enhancement that we made is to add new construction of power plants. Per your question, "addition" would be the right word. This is clarified in the text.

**VP7** L2: Why project to 2015 and not project emissions to 2016?

The NIER (National Institute of Environmental Research) of Korea generates a "Present Version Inventory," for their air quality forecasting, by projecting the base year inventory for three years (i.e. 2015). In this simulation, we use that version of the inventory. We have clarified that NIER provided the projected emissions, and that we did not project the emissions.

**VP8** L8-10: This statement would be stronger if a reference is cited

Reference to de Foy et al. (2014) is now included.

**VL10-12:** The ratio of NO<sub>2</sub> to NO<sub>x</sub> is time-dependent and spatially varying, depending primarily on JNO<sub>2</sub> and O<sub>3</sub>. This should at least be noted.

## Updated

**VL21:** please clarify that you are referring to ERA-Interim winds

## Clarified

✓P9: L19-34: The chemical lifetime of NO<sub>x</sub> is impacted by uncertainties in the simulations VOC concentrations and type, OH, RO<sub>2</sub> and R(O)O<sub>2</sub> radicals. As an example, simulated atmospheric concentrations of aromatic compounds in Seoul are much smaller than observed during KORUS-AQ. An underestimate of aromatics would certainly have a large impact on peroxyacyl and alkyl nitrate formation, and should enhance the effective NO<sub>x</sub> lifetime in the near-field.

This has been updated. Romer et al., (2016) has now been cited to support this.

✓Without further justification or analysis, I don't think the comparison of emission timing is all that helpful. We would expect a different time-of-day profile of NO<sub>x</sub> emissions in Korea and USA given that the source mix of NO<sub>x</sub> is different. Emissions timing can be listed as an uncertainty without devoting an entire figure to it (Fig. 4).

The emission timing is critical to the conclusion of this paper. We are suggesting that the timing of emissions can yield a large amount of uncertainty when evaluating emission inventories with satellite data. Thus, we still include this figure.

✓P10: L20-21: please report the correlation coefficients here and refer to Figure 6.

Included

✓L32: If archived, please compute the chemical lifetime of NO<sub>x</sub> in the model based on all NO<sub>y</sub> species.

This was not archived.

✓P11: L1-4: From where do the uncertainty estimates affecting the analysis originate?

Please reference Lu et al., (2015). We have added the citation here.

✓L3-4: "Only the latter three terms are used to calculate the uncertainty of the NO<sub>2</sub> lifetime" Why? The NO<sub>x</sub> to NO<sub>2</sub> ratio has a large impact on the NO<sub>2</sub> (NO<sub>x</sub>) chemical lifetime as NO removal tends to be much slower than NO<sub>2</sub> removal.

Please reference Lu et al., (2015). We have added the citation here.

✓L6-7: Why choose a radius of 40 km when the rotated plume domain width is 250 km? It seems a bit arbitrary as distance can be adjusted to improve the comparison of top-down results with bottom-up inputs.

An assumption with this method is that all of the NO<sub>x</sub> emissions are clustered near a single point. The radius of 40 km from the city center is chosen because it encompasses an area which includes the highest NO<sub>x</sub> emission sources, but very little of the emissions from more rural areas, which are contributing to the background NO<sub>2</sub>. A radius much larger than 40 km would be inappropriate.

For the calculation of the OMI line densities, we apply a 120 km radius (we are unsure where you saw the number 250 as it is not in the original manuscript). By doing so, we are assuming that emissions between a radius of 40 km and 120 km are contributing to the background. This is an assumption of the top-down method. Figure 7 confirms that this is a valid assumption.

**VP11:** L30-31: I recommend completing a validation analysis of more than two days' worth of simulations.

This is now included. Please refer to Figures 9 & 10.

**VP12:** L24-25: "This is because the lifetime calculation is extremely sensitive to the accuracy of the wind direction." Given that top-down inference of lifetime, emissions and estimates of background NO<sub>2</sub> are directly linked in the EMG analysis, the above statement is also true for inference of top-down emissions and background NO<sub>2</sub>. Is this "extreme sensitivity" appropriately characterized by the 30% error estimate reported on P11, L3? Please move this discussion from conclusions section on P12 to error estimate discussion early on P11 and provide a more detailed accounting.

As suggested, this has been moved to Section 3.6.2. A reference is now also cited, de Foy et al. (2014), which describes in detail the uncertainty analysis.

# A top-down assessment using OMI NO<sub>2</sub> suggests an underestimate in the NO<sub>x</sub> emissions inventory in Seoul, South Korea during KORUS-AQ

5 Daniel L. Goldberg<sup>\*,1,2</sup>, Pablo E. Saide<sup>3</sup>, Lok N. Lamsal<sup>4,5</sup>, Benjamin de Foy<sup>6</sup>, Zifeng Lu<sup>1,2</sup>, Jung-Hun Woo<sup>7</sup>, Younha Kim<sup>7</sup>, Jinseok Kim<sup>7</sup>, Meng Gao<sup>8</sup>, Gregory Carmichael<sup>9</sup>, and David G. Streets<sup>1,2</sup>

<sup>1</sup>Energy Systems Division, Argonne National Laboratory, Argonne, IL 60439 USA

<sup>2</sup>Consortium for Advanced Science and Engineering, University of Chicago, Chicago, IL 60637, USA

10 <sup>3</sup>Department of Atmospheric and Oceanic Sciences, Institute of the Environment and Sustainability, University of California – Los Angeles, Los Angeles, CA 90095, USA

<sup>4</sup>Goddard Earth Sciences Technology and Research, Universities Space Research Association, Columbia, MD 21046, USA

<sup>5</sup>NASA Goddard Space Flight Center, Code 614, Greenbelt, MD 20771, USA

15 <sup>6</sup>Department of Earth and Atmospheric Sciences, Saint Louis University, St. Louis, MO 63108, USA

<sup>7</sup>Konkuk University, 05029 Seoul, South Korea

<sup>8</sup>School of Engineering and Applied Sciences, Harvard University, Cambridge, MA 02138, USA

<sup>9</sup>Department of Chemical and Biochemical Engineering, University of Iowa, Iowa City, IA 52242, USA

*Correspondence to:* Daniel L. Goldberg ([dgoldberg@anl.gov](mailto:dgoldberg@anl.gov))

20

**Abstract.** In this work, we investigate the NO<sub>x</sub> emissions inventory in Seoul, South Korea using a regional **NASA** Ozone Monitoring Instrument (OMI) NO<sub>2</sub> product derived from the standard NASA product. We first develop a regional OMI NO<sub>2</sub> product by re-calculating the air mass factors using a high-resolution (4 × 4 km<sup>2</sup>) WRF-Chem model simulation, which better captures the NO<sub>2</sub> ~~shape-profiles~~profile shapes in urban regions. We then apply a model-derived spatial averaging kernel to further downscale the retrieval and account for the sub-pixel variability. These two modifications yield OMI NO<sub>2</sub> values in the regional product that are 1.37 larger in the Seoul metropolitan region and >2 times larger near ~~large industrial~~substantial point sources. These two modifications also yield an OMI NO<sub>2</sub> product that is in better agreement with the Pandora NO<sub>2</sub> spectrometer measurements acquired during the Korea U.S.-Air Quality (KORUS-AQ) field campaign. NO<sub>x</sub> emissions are then derived for the Seoul metropolitan area during the KORUS-AQ field campaign using a top-down approach with the standard and regional NASA OMI NO<sub>2</sub> products. We first apply the top-down approach to a model simulation to ensure that the method is appropriate: the WRF-Chem simulation utilizing the bottom-up emission inventory yields a NO<sub>x</sub> emission rate of 227 ± 94 kton/yr, while the bottom-up inventory itself yields a NO<sub>x</sub> emission rate of 198 kton/yr. Using the top-down approach on the regional OMI NO<sub>2</sub> product, we derive the NO<sub>x</sub> emissions rate from Seoul to be 484 ± 201 kton/yr, and a 353 ± 146 kton/yr NO<sub>x</sub> emissions rate using the standard NASA OMI NO<sub>2</sub> product. This suggests an underestimate of 53% and 36% using the regional and standard NASA OMI NO<sub>2</sub> products respectively. To supplement this finding, we compare the NO<sub>2</sub> and NO<sub>y</sub> simulated by WRF-Chem to observations of the same quantity acquired by aircraft and find a model underestimate. When NO<sub>x</sub> emissions in the WRF-Chem model are ~~doubled~~increased by a factor of 2.13 in the Seoul metropolitan area, there is better agreement with KORUS-AQ aircraft observations and the re-calculated OMI NO<sub>2</sub> tropospheric columns. Finally, we show that by using a WRF-Chem simulation with an updated emissions inventory to re-calculate the AMF, there are small differences (~~40–20~~~8%) in OMI NO<sub>2</sub> compared to using the original WRF-Chem simulation to derive the AMF. This suggests that changes in model resolution have a larger effect on the AMF

40

calculation than modifications to the Korean emissions inventory. Although the current work is focused on South Korea using OMI, the methodology developed in this work can be applied to other world regions using TROPOMI and future satellite datasets (e.g., GEMS and TEMPO) to produce high-quality region-specific top-down NO<sub>x</sub> emission estimates.

## 1 Introduction

Nitrogen oxides ( $\text{NO}_x \equiv \text{NO} + \text{NO}_2$ ) are a group of reactive trace gases that are toxic to human health and can transform in the atmosphere into other noxious chemical species. ~~During ideal atmospheric conditions~~ In the presence of abundant volatile organic compounds and strong sunlight,  $\text{NO}_x$  can ~~photolyze~~ participate in a series of chemical reactions to ~~create~~ accelerate the production of  $\text{O}_3$ , another toxic air pollutant with a longer atmospheric lifetime.  $\text{NO}_x$  can also transform into particulate nitrate, a component of fine particulate matter ( $\text{PM}_{2.5}$ ), ~~another~~ an additional health hazard. When fully oxidized in the atmosphere,  $\text{NO}_x$  transforms into  $\text{HNO}_3$ , a key contributor to acid rain. There are some biogenic ~~sources~~ emissions of  $\text{NO}_x$  (e.g., lightning), but the majority of the  $\text{NO}_x$  ~~in our atmosphere today is emitted by~~ emissions are from anthropogenic sources (van Vuuren et al., 2011).

~~There is a rich legacy of  $\text{NO}_2$  measurements by remote sensing instruments (Burrows et al., 1999).  $\text{NO}_2$  is one of the easiest trace gases to observe from space because it has strong absorption features within the 400–465 nm wavelength region (Vandaele et al., 1998). One of these instruments is the Dutch-Finnish Ozone Monitoring Instrument (OMI), which measures the absorption of solar backscatter in the UV-visible spectral range.  $\text{NO}_2$  can be observed from space because it has strong absorption features within the 400–465 nm wavelength region (Vandaele et al., 1998).~~ By comparing observed spectra with a reference spectrum, the amount of  $\text{NO}_2$  in the atmosphere between the instrument in low-earth orbit and the surface can be derived; this technique is called differential optical absorption spectroscopy (DOAS) (Platt, 1994).

Tropospheric  $\text{NO}_2$  column contents from OMI have been used to estimate  $\text{NO}_x$  emissions from various areas around the globe (Streets et al., 2013; Miyazaki et al., 2017) including North America (Boersma et al., 2008; Lu et al., 2015), Asia (Zhang et al., 2008; Han et al., 2015; Kuhlmann et al., 2015; Liu et al., 2017), the Middle East (Beirle et al., 2011), and Europe (Huijnen et al., 2010; Curier et al., 2014). It has also been used to produce and validate  $\text{NO}_x$  emission estimates from sectors such as soil (Hudman et al., 2010; Vinken et al., 2014a; Rasool et al., 2016), lightning (Allen et al., 2012; Liaskos et al., 2015; Pickering et al., 2016; Nault et al., 2017), power plants (de Foy et al., 2015), aircraft (Pujadas et al., 2011), marine vessels (Vinken et al., 2014b; Boersma et al., 2015), and urban centers (Lu et al., 2015; Canty et al., 2015; Souri et al., 2016).

With a pixel resolution varying from  $13 \times 24 \text{ km}^2$  to  $26 \times 128 \text{ km}^2$ , the OMI sensor was developed for global to regional scale studies rather than for individual urban areas. Even at the highest spatial resolution of  $13 \times 24 \text{ km}^2$ , the sensor has difficulty observing the fine structure of  $\text{NO}_2$  plumes at or near the surface (e.g., highways, power plants, factories, etc.) (Chen et al., 2009; Ma et al., 2013; Flynn et al., 2014), which are often less than 10 km in width (Heue et al., 2008). This can lead to a spatial averaging of pollution (Hilboll et al., 2013). A temporary remedy, until higher spatial resolution satellite instruments are operational, is to use a regional air quality simulation to estimate the sub-pixel variability of OMI pixels. Kim et al. (2016) utilize the spatial variability in a regional air quality model to spatially downscale OMI  $\text{NO}_2$  measurements using a spatial averaging kernel. The spatial averaging kernel technique has shown to increase the OMI  $\text{NO}_2$  signal within urban areas, which is in better agreement with observations in these regions (Goldberg et al., 2017).

Furthermore, the air mass factor and surface reflectance used in obtaining the global OMI NO<sub>2</sub> retrievals are at a coarse spatial resolution (Lorente et al. 2017; Kleipool et al., 2008). While appropriate for a global operational retrieval, this is known to cause an underestimate in the OMI NO<sub>2</sub> signal in urban regions (Russell et al., 2011). The air mass factors in operational OMI NO<sub>2</sub> are calculated using NO<sub>2</sub> ~~shape profiles~~ profile shapes that are provided at a 1.25° × 1° spatial resolution in the NASA product (Krotkov et al. 2017) and 2° × 3° spatial resolution in the DOMINO product (Boersma et al., 2011). Developers of the NASA product provide scattering weights and additional auxiliary information so that users can develop their own tropospheric vertical column product a posteriori (Lamsal et al. 2015). Several users have re-calculated the air mass factor using a regional air quality model (Russell et al., 2011; Kuhlmann et al. 2015; Lin et al., 2015; Goldberg et al., 2017), which can better capture the NO<sub>2</sub> ~~shape profiles~~ profile shapes in urban regions. Other techniques to improve the air mass factor involve correcting for the surface pressure in mountainous terrain (Zhou et al., 2009) and accounting for small-scale heterogeneities in surface reflectance (Zhou et al., 2010; Vasilkov et al., 2017). These a posteriori products have better agreement with ground-based spectrometers measuring tropospheric vertical column contents (Goldberg et al., 2017). When available, observations from aircraft can constrain the NO<sub>2</sub> ~~shape profiles~~ profile shapes used in the air mass factor calculation (Goldberg et al., 2017).

In this paper, we apply both techniques (the spatial averaging kernel and an air mass factor adjustment) to develop a regional OMI NO<sub>2</sub> product for South Korea. We then use the regional product with only the air mass factor adjustment to derive NO<sub>x</sub> emission estimates for the Seoul metropolitan area using an exponentially modified Gaussian (EMG) function (Beirle et al., 2011; Valin et al., 2013; de Foy et al., 2014; Lu et al., 2015); the methodology is described in-depth in Section 2.5.

## 2 Methods

### 2.1 OMI NO<sub>2</sub>

OMI has been operational on NASA's Earth Observing System (EOS) Aura satellite since October 2004 (Levelt et al., 2006). The satellite follows a sun-synchronous, low-earth (705 km) orbit with an equator overpass time of approximately 13:45 local time. OMI measures total column amounts in a 2600 km swath divided into 60 unequal area "field-of-views", or pixels. At nadir (center of the swath), pixel size is 13 × 24 km<sup>2</sup>, but at the swath edges, pixels can be as large as 26 × 128 km<sup>2</sup>. In a single orbit, OMI measures approximately 1650 swaths and achieves daily global coverage over 14 – 15 orbits (99 minutes per orbit). Since June 2007, there has been a partial blockage of the detector's full field of view, which has limited the number of valid measurements by blocking consistent rows of data; this is known in the community as the row anomaly (Dobber et al., 2008): <http://projects.knmi.nl/omi/research/product/rowanomaly-background.php>.

OMI measures radiance data between the instrument's detector and the Earth's surface. Comparison of these measurements with a reference spectrum (i.e., DOAS technique), enables the calculation of the total slant column density (SCD), which represents an integrated trace gas abundance from the sun to the surface and back to the instrument's detector, passing through the atmosphere twice. For tropospheric air quality studies, vertical column

density (VCD) data are more useful. This is done by subtracting the stratospheric slant column from the total (tropospheric + stratospheric) slant column and dividing by the tropospheric air mass factor (AMF), which is defined as the ratio of the SCD to the VCD, as shown in Eq. (1):

$$VCD_{trop} = \frac{SCD_{total} - SCD_{strat}}{AMF_{trop}}, \text{ where } AMF_{trop} = \frac{SCD_{trop}}{VCD_{trop}} \quad (1)$$

5 The tropospheric AMF has been derived to be a function of the optical atmospheric/surface properties (viewing and solar angles, surface reflectivity, cloud radiance fraction, and cloud height) and a priori ~~shape~~-profile ~~shape~~ (Palmer et al., 2001; Martin et al., 2002) and can be calculated as follows (Lamsal et al., 2014) in Eq. (2):

$$AMF_{trop} = \frac{\sum_{n=surface}^{tropopause} SW_n \times x_{an}}{\sum_{n=surface}^{tropopause} x_{an}} \quad (2)$$

10 where  $x_a$  is the partial column. The optical atmospheric/surface properties in the NASA retrieval are characterized by the scattering weight and are calculated by a forward radiative transfer model (TOMRAD), which are output as a look-up table. The scattering weights are then adjusted real-time depending on observed viewing angles, surface albedo, cloud radiance fraction, and cloud pressure.

For this study, we follow previous studies (e.g., Palmer et al., 2001, Martin et al., 2002, Boersma et al., 2011, Bucsela et al., 2013) and assume that scattering weights and trace gas profile shapes are independent. The a priori trace gas profile shapes ( $x_a$ ) must be provided by a model simulation. In an operational setting, NASA uses a monthly-averaged and year-specific Global Model Initiative (GMI) global simulation with a spatial resolution of  $1.25^\circ \text{ lon} \times 1^\circ \text{ lat}$  (~110 km  $\times$  110 km in the mid-latitudes) to provide the a priori ~~shape profiles~~profile shapes.

We derive tropospheric VCDs using a priori NO<sub>2</sub> ~~shape profiles~~profile shapes from a regional WRF-Chem simulation. A full description of this methodology can be found in Goldberg et al. (2017); it is also described in brief in section 2.1.1. We filter the Level 2 OMI NO<sub>2</sub> data to ensure only valid pixels are used. Daily pixels with solar zenith angles  $\geq 80^\circ$ , cloud radiance fractions  $\geq 0.5$ , or surface albedo  $\geq 0.3$  are removed as well as the five largest pixels at the swath edges (i.e., pixel numbers 1 – 5 and 56 – 60). Finally, we remove any pixel flagged by NASA including pixels with NaN values, ‘XTrackQualityFlags’  $\neq 0$  or 255 (RA flag), or ‘VcdQualityFlags’  $> 0$  and least significant bit  $\neq 0$  (ground pixel flag).

### 25 2.1.1 OMI-WRF-Chem NO<sub>2</sub>

We modify the air mass factor in the OMI NO<sub>2</sub> retrieval based on the vertical profiles from a high spatial ( $4 \times 4 \text{ km}^2$ ) resolution WRF-Chem simulation. The vertical profiles are scaled based on a comparison with in situ aircraft observations; this accounts for any consistent biases in the model simulation. For example, if the aircraft observations show that mean NO<sub>2</sub> concentrations between 0 - 500 m are low by 50%, then we scale the modeled NO<sub>2</sub> in this altitude bin by this same amount. To re-calculate the air mass factor for each OMI pixel, we first compute sub-pixel air mass

factors for each WRF-Chem model grid cell, using the same method as outlined in Goldberg et al. (2017). The sub-pixel air mass factor for each WRF-Chem grid cell is a function of the modelled NO<sub>2</sub> ~~shape~~-profile shape and the scattering weight calculated by a radiative transfer model. We then average all sub-pixel air mass factors within an OMI pixel (usually 10-100) to generate a single tropospheric air mass factor for each individual OMI pixel. This new  
5 air mass factor is used to convert the total slant column into a total vertical column using Equation 1. Model outputs were sampled at the local time of OMI overpass. For May 2016, we used daily NO<sub>2</sub> profiles and terrain pressures (e.g., (Zhou et al., 2009, Laughner et al., 2016)) to re-calculate the AMF. For other months and years, we used May 2016 monthly mean values of NO<sub>2</sub> and tropopause pressures for the a priori profiles, which are used in the calculation of the AMF.

10 Once the tropospheric vertical column of each OMI pixel was re-calculated, the product was oversampled (de Foy et al., 2009; Russell et al., 2010) for April – June over a 3-year period (2015-2017; 9 months total). During this timeframe, there are approximately 9 valid OMI NO<sub>2</sub> pixels per month over any given location on the Korean peninsula. In the top-down emissions derivation, we use all nine-months of OMI data for the analysis.

## 2.2 NO<sub>2</sub> observations during KORUS-AQ

15 We use in situ NO<sub>2</sub> observations from the KORUS-AQ field campaign to test the regional satellite product. KORUS-AQ was a joint Korea-US field experiment designed to better understand the trace gas and aerosol composition above the Korean peninsula using aircrafts, ground station networks, and satellites. The campaign took place between May 1, 2016 and June 15, 2016 and measurements were primarily focused in the Seoul Metropolitan Area. In this paper, we utilize data acquired by the ground-based Pandora spectrometer network, ~~and~~ the thermally dissociated laser-  
20 induced fluorescence NO<sub>2</sub> instrument on DC-8 aircraft, and the chemiluminescence NO<sub>y</sub> instrument on the DC-8 aircraft (NO<sub>y</sub> = NO + NO<sub>2</sub> + HNO<sub>3</sub> + 2×N<sub>2</sub>O<sub>5</sub> + peroxy nitrates + alkyl nitrates + ...). KORUS-AQ observations were retrieved from the online data archive: <http://www-air.larc.nasa.gov/cgi-bin/ArcView/korusaq>. A further description of this field campaign can be found in the KORUS-AQ White Paper ([https://espo.nasa.gov/korus-aq/content/KORUS-AQ\\_Science\\_Overview\\_0](https://espo.nasa.gov/korus-aq/content/KORUS-AQ_Science_Overview_0)).

### 2.2.1 Pandora NO<sub>2</sub> data

Measurements of total column NO<sub>2</sub> from the Pandora instrument (Herman et al., 2009; Herman et al., 2018) are used to evaluate the OMI NO<sub>2</sub> satellite products. The Pandora instrument is a stationary, ground-based, sun-tracking spectrometer, which measures direct sunlight in the UV-Visible spectral range (280-525 nm) with a sampling period of 90 seconds. The Pandora spectrometer measures total column NO<sub>2</sub> using a DOAS technique similar to OMI. A  
30 distinct advantage of the Pandora instrument is that it does not require complex assumptions for converting slant columns into vertical columns, compared to zenith sky measurements (e.g., MAX-DOAS).

Valid OMI NO<sub>2</sub> pixels are matched spatially and temporally to Pandora total column NO<sub>2</sub> observations. To smooth the data and eliminate brief small-scale plumes that would be undetectable by a satellite, we average the Pandora

observations over a two hour period ( $\pm$  one hour of the overpass time) before matching to the OMI NO<sub>2</sub> data (Goldberg et al., 2017). During May 2016, there were seven Pandora NO<sub>2</sub> spectrometers operating during the experiment (five instruments were situated within the Seoul metropolitan area and their locations are shown in Figure 5); this corresponded to fifty instances in which valid Pandora NO<sub>2</sub> observations matched valid OMI NO<sub>2</sub> column data.

## 5 2.2.2 DC-8 aircraft data

We compare the model simulation to in situ NO<sub>2</sub> data gathered by the [UC-Berkeley](#) Cohen group (Thornton et al., 2000; Day et al, 2002) on the DC-8 aircraft. The instrument quantifies NO<sub>2</sub> via laser-induced fluorescence at 585 nm. This instrument does not have the same positive bias as chemiluminescence NO<sub>2</sub> detectors, so there is no need to modify NO<sub>2</sub> concentrations by applying an empirical equation (e.g., Lamsal et al., 2008). [We also compare the model simulation to chemiluminescence NO<sub>y</sub> data gathered by the NCAR Weinheimer group \(Ridley et al., 2004\)](#)

We utilize one-minute averaged DC-8 data from all fourteen flights during May – June 2016. A typical flight path included several low-altitude spirals over the Seoul Metropolitan Area and a long-distance transect over the Korean peninsula or the Yellow Sea. One-minute averaged data is already pre-generated in the data archive. Hourly output from the model simulation is spatially and temporally matched to the observations. We then bin the data into different altitude ranges for our comparison.

## 2.3 WRF-Chem model simulation

For the high-resolution OMI NO<sub>2</sub> product, we use a regional simulation of the Weather Research & Forecasting (Skamarock et al., 2008) coupled to Chemistry (WRF-Chem) (Grell et al., 2005) in forecast mode prepared for flight planning during the KORUS-AQ field campaign. The forecast simulations were performed daily and used National Centers for Environmental Prediction Global Forecast System (<https://rda.ucar.edu/datasets/ds084.6/>) meteorological initial and boundary conditions from the 06 UTC cycle. Initial conditions for aerosols and gases were obtained from the previous forecasting cycle, while Copernicus Atmosphere Monitoring Service (Inness et al., 2015) forecasts were used as boundary conditions. WRF-Chem was configured with two domains, with 20 km and 4 km grid-spacing. The 20 km domain included the major sources for trans-boundary pollution impacting the Korean peninsula (deserts in China and Mongolia, wild-fires in Siberia and anthropogenic sources from China). The 4 km domain provided a high-resolution simulation where detailed local sources could be modeled and where the KORUS-AQ flight tracks were contained. The inner domain was started 18 hours after the outer domain, and was simulated for 33 hours (00UTC from day 1 to 9 UTC of day 2 of the forecast); output was saved hourly. The last 24 hours of each inner domain daily forecast over the course of KORUS-AQ were selected to allow spin-up from the outer domain and were used in the analysis presented here.

WRF-Chem was configured with 4 bin MOSAIC aerosols (Zaveri et al., 2008), a reduced hydrocarbon trace gas chemical mechanism (Pfister et al., 2014) including simplified secondary organic aerosol formation (Hodzic and Jimenez, 2011), and with capabilities to assimilate satellite aerosol optical depth both from low-earth orbiting and

geostationary satellites (Saide et al., 2013, 2014), ~~which to our knowledge is the first near real time application of geostationary satellite data assimilation for air quality forecasts.~~

## 2.4 Emission Inventory

5 The WRF-Chem simulation was driven by emissions developed by Konkuk University. Monthly emissions for South Korea were developed using the projected 2015 Korean national emissions inventory, Clean Air Policy Support System (CAPSS) provided by the National Institute of Environmental Research of Korea and with enhancements by Konkuk University, which primarily includes the addition of new power plants. The projected CAPSS 2015 emissions were estimated based on CAPSS 2012 and 3-year growth factors. Since the base year of the inventory is 2012, observed emissions from the post-2013 Large Point Source inventory were not included. Emissions from China and  
10 North Korea were taken from the Comprehensive Regional Emissions for Atmospheric Transport Experiments (CREATE) v3.0 emissions inventory. In order to project the year 2010 emissions to 2015, the latest energy statistics from the International Energy Agency (<http://www.iaea.org/weo2017/>) and the China Statistical Yearbook 2016 (<http://www.stats.gov.cn/tjsj/ndsj/2016/indexeh.htm>) were used to update the growth of fuel activities. In addition, the new emissions control policies in China, which were compiled by the International Institute for Applied Systems  
15 Analysis, were applied to consider efficiencies of emissions control (van der A et al., 2017).

Emissions were first processed to the monthly time-scale at a spatial resolution of 3 km in South Korea and 0.1° for the rest of Asia using SMOKE-Asia (Woo et al., 2012). Information from GIS, such as population, road network, and land cover, were applied to generate gridded emissions from the region-based (17 metropolitan and provincial boundaries of South Korea) emissions. The GIS-based population and regional boundary data compiled by the  
20 Ministry of Interior and Safety (<http://www.mois.go.kr/frt/sub/a05/totStat/>), and land cover data compiled by the Ministry of Environment (<https://egis.me.go.kr/>) were used to generate population and land cover based spatial surrogates. The Road and Railroad network data compiled by The Korea Transport Institute were used to generate spatial surrogates for onroad and nonroad emissions (<https://www.koti.re.kr/>). The emissions were downscaled temporally from monthly to hourly and spatially re-allocated to 4 km over South Korea and 20 km over the rest of  
25 East Asia using the University of Iowa emission pre-processor (EPRES).

Biogenic emissions are included using the on-line Model of Emissions of Gases and Aerosols from Nature (MEGAN) model version 2; there are no NO<sub>x</sub> emissions from MEGAN. For this simulation, the lightning NO<sub>x</sub> parameterization was turned off. For wildfires we used the Quick Fire Emissions Dataset (QFED2), but there were only isolated, small fires in South Korea during this timeframe.

## 30 2.5 Exponentially Modified Gaussian Fitting Method

An exponentially modified Gaussian (EMG) function is fit to a collection of NO<sub>2</sub> plumes observed from OMI in order to determine the NO<sub>2</sub> burden and lifetime from the Seoul metropolitan area. The original methodology, proposed by Beirle et al. (2011), involves the fitting of OMI NO<sub>2</sub> line densities to an EMG function. OMI NO<sub>2</sub> line densities are

the integral of OMI NO<sub>2</sub> retrieval perpendicular to the path of the plume; the units are mass per distance. We define integration length scale as the across plume width. The across plume width is dependent on the NO<sub>2</sub> plume size and can vary between 10 km (for small point sources) to 240 km (for large urban areas). Visual inspection of the rotated oversampled OMI NO<sub>2</sub> ~~plume,plumes~~ is the best way to determine the spatial extent of the emission sources (Lu et al. 2015).

The EMG model is expressed as Equation (3):

$$OMI\ NO_2\ Line\ Density = \alpha \left[ \frac{1}{x_o} \exp\left(\frac{\mu}{x_o} + \frac{\sigma^2}{2x_o^2} - \frac{x}{x_o}\right) \Phi\left(\frac{x-\mu}{\sigma} - \frac{\sigma}{x_o}\right) \right] + \beta \quad (3)$$

where  $\alpha$  is the total number of NO<sub>2</sub> molecules observed near the hotspot, excluding the effect of background NO<sub>2</sub>,  $\beta$ ;  $x_o$  is the e-folding distance downwind, representing the length scale of the NO<sub>2</sub> decay;  $\mu$  is the location of the apparent source relative to the city center;  $\sigma$  is the standard deviation of the Gaussian function, representing the Gaussian smoothing length scale;  $\Phi$  is the cumulative distribution function. Using the ‘curvefit’ function in IDL, we determine the five unknown parameters:  $\alpha$ ,  $x_o$ ,  $\sigma$ ,  $\mu$ ,  $\beta$  based on the independent (distance;  $x$ ) and dependent (OMI NO<sub>2</sub> line density) variables.

Using the mean zonal wind speed,  $w$ , of the NO<sub>2</sub> line density domain, the mean effective NO<sub>2</sub> lifetime  $\tau_{effective}$  and the mean NO<sub>x</sub> emissions can be calculated from the fitted parameters  $x_o$  and  $\alpha$ . The wind speed and direction are obtained from the ERA-Interim re-analysis project (Dee et al., 2011), instead of the WRF simulation because the WRF simulation is a forecast. We use the averaged wind fields of the bottom eight levels of the re-analysis (i.e., from the surface to ~500 m). Only days in which the wind speeds are > 3 m/s are included in this analysis, because NO<sub>2</sub> decay under this condition is dominated by chemical removal, not variability in the winds (de Foy et al., 2014). The factor of 1.33 is the mean column-averaged NO<sub>x</sub> / NO<sub>2</sub> ratio in the WRF-Chem model simulation for the Seoul metropolitan area during the mid-afternoon. The NO<sub>x</sub> / NO<sub>2</sub> ratio is time-dependent, spatially varying and is primarily a function of the localized j(NO<sub>2</sub>) and O<sub>3</sub> concentration.

$$NO_x\ Emissions = 1.33 \left( \frac{\alpha}{\tau_{effective}} \right), \text{ where } \tau_{effective} = \frac{x_o}{w} \quad (4)$$

The NO<sub>2</sub> plume concentration is a function of the emission source strength, wind speed, and wind direction. Originally, the method separated all NO<sub>2</sub> plumes by wind direction, and fit an EMG function to NO<sub>2</sub> in eight wind directions (Beirle et al., 2011; Ialongo et al., 2014; Liu et al., 2016). Newer methodologies rotate the plumes so that all plumes are in the same direction (Valin et al., 2013; de Foy et al., 2014; Lu et al., 2015). This process increases the signal-to-noise ratio and generates a more robust fit. In this work, we filter OMI NO<sub>2</sub> data and rotate the NO<sub>2</sub> plumes and as described in Lu et al. (2015), so that all plumes are decaying in the same direction. We rotate the retrieval based on the re-analyzed 0-500 m wind speed direction from the ERA-Interim. In doing so, we develop a re-gridded satellite product in an x-y coordinate system, in which the urban plume is aligned along the x-axis. Following de Foy et al. (2014) and Lu et al. (2015), we only use days in which the ERA-Interim wind speeds are > 3 m/s because there is

more direct plume transport and less plume meandering on days with stronger winds; this yields more robust NO<sub>x</sub> emission estimates. We fit an EMG function to the line density as function of the horizontal distance. This yields a single value at each point along the x-direction.

### 3 Results

5 In this section, we describe the regional high-resolution satellite product and our validation efforts. All OMI NO<sub>2</sub> results presented here are vertical column densities. First, we show a continental snapshot of OMI NO<sub>2</sub> (OMI-Standard) over East Asia using the standard NASA product. Then, we show a regional NASA OMI NO<sub>2</sub> satellite product (OMI-Regional) using AMFs generated from the WRF-Chem a priori NO<sub>2</sub> profiles. We compare the OMI-Regional product with NO<sub>2</sub> VCDs from the original WRF-Chem simulation. We evaluate the OMI-Regional product  
10 by comparing to KORUS-AQ observations. Finally, we use the OMI-Standard and OMI-Regional products to estimate NO<sub>x</sub> emissions from the Seoul metropolitan area.

#### 3.1 OMI NO<sub>2</sub> in East Asia

Oversampled OMI NO<sub>2</sub> for May – September 2015 – 2017 (15 months total) in East Asia and the 4 km WRF-Chem model domain area ~~and the US is~~ shown in Figure 1. The OMI NO<sub>2</sub> signals in East Asia over major metropolitan areas  
15 are 3 to 5 times larger than over similarly sized cities in the US (Krotkov et al., 2016). This is in despite of recent NO<sub>x</sub> reductions in China since 2011 (de Foy et al., 2016; Souri et al., 2017; Zheng et al., 2018). OMI has observed a recent decrease in the NO<sub>2</sub> burden in the immediate Seoul, South Korea metropolitan area, but an increase in areas just outside the city center (Duncan et al., 2016). Oversampled values greater than  $8 \times 10^{15}$  molecules per cm<sup>2</sup> are still consistently seen in East Asia, while they are non-existent in the US during the warm season.

#### 20 3.2 Calculation of new OMI tropospheric column NO<sub>2</sub>

In Figure 2, we plot the OMI-Standard and OMI-Regional products over South Korea. The top center panels shows a regional product in which only the air mass factor correction is applied (AMF). The bottom center panels shows a regional product in which the air mass factor correction and spatial averaging kernel are applied (AMF+SK). The regional product yields larger OMI NO<sub>2</sub> values throughout the majority of the Korean peninsula. Areas near major  
25 cities (e.g. Seoul), power plants, steel mills, and cement kilns have OMI NO<sub>2</sub> values that are >1.25 times larger in the regional AMF product and >2 times larger in the regional AMF+SK product. There are two reasons for the larger OMI NO<sub>2</sub> signals: the air mass factors in polluted regions are now smaller (Russell et al., 2011; Goldberg et al., 2017) and the spatial weighting kernel allocates a large portion of the OMI NO<sub>2</sub> signal into a smaller region (Kim et al., 2016). ~~There are small decreases in the northeastern Korean peninsula due to an increase in the air mass factors in these regions.~~  
30

### 3.3 OMI-Regional vs. WRF-Chem

We now compare the OMI-Regional product to tropospheric vertical columns from the WRF-Chem model simulation directly. In Figure 3, we compare the regional satellite product (AMF+SK) to the WRF-Chem simulation over the Korean peninsula. In ~~all-most~~ areas, the modeled tropospheric column NO<sub>2</sub> is of smaller magnitude than inferred by the satellite. In the area within 40 km of the Seoul city center, modeled tropospheric vertical columns are 44% smaller than observed tropospheric vertical column in the regional AMF+SK product. We posit ~~three-four~~ reasons as to why the model simulation calculates columns that are consistently smaller. First, WRF-Chem uses a reduced hydrocarbon gas-phase chemical mechanism. This fast-calculating mechanism implemented in WRF-Chem for regional climate assessments (Pfister et al., 2014) and used during KORUS-AQ for forecasting does not quickly recycle alkyl nitrates back to NO<sub>2</sub>; this will cause NO<sub>2</sub> to be too low. While an underestimate of the chemical conversion to NO<sub>2</sub> in WRF-Chem is a contributor to the underestimate, it likely does not account for the entire discrepancy; Canty et al., (2015) suggests that by shortening the lifetime of alkyl nitrates in the chemical mechanism, NO<sub>2</sub> will increase by roughly 3% in urban areas and 18% in rural areas. Second, an underestimate in VOC emissions would have an impact on peroxyacyl and alkyl nitrate formation, and should enhance the effective NO<sub>x</sub> lifetime (Romer et al., 2016). ~~Second~~Third, the temporal allocation of NO<sub>x</sub> emissions in this WRF-Chem simulation is such that the early afternoon rate (between 12:00 – 14:00 local time) is approximately equal to 24-hour averaged rate (Figure 4). For comparison, using SMOKE in the eastern US yields an early afternoon emission rate that is 1.35 larger than the 24-hour averaged emission rate. Lastly, the remaining difference will likely be due to an underestimate in the emissions inventory.

#### 3.3.14 Comparing WRF-Chem to Aircraft Measurements

When comparing the model simulation to in situ observations from the UC-Berkeley NO<sub>2</sub> instrument aboard the aircraft, we find that NO<sub>2</sub> concentrations are substantially larger than the model when spatially and temporally co-located in the immediate Seoul metropolitan area (Figure 5). The comparison isolates the NO<sub>2</sub> within the lowermost boundary layer as the primary contributor to the tropospheric column underestimate. When comparing aircraft NO<sub>2</sub> to modeled NO<sub>2</sub> in other areas of the Korean peninsula, the underestimate is ~~consistently~~ smaller. ~~This suggests a larger underestimate in the NO<sub>x</sub> emissions inventory in the immediate Seoul metropolitan area.~~

When comparing the model simulation of NO<sub>y</sub> to observations of the same quantity observed from the aircraft, we find a similarly large underestimate. NO<sub>y</sub> observed on the aircraft is roughly a factor of two larger at all altitudes below 2 km. This suggests that errors in NO<sub>2</sub> recycling (NO<sub>2</sub> ↔ NO<sub>y</sub>) are not the main cause of the NO<sub>2</sub> discrepancies seen in the satellite and aircraft comparison. Instead, there must be errors in the NO<sub>y</sub> production (i.e., NO<sub>x</sub> emission rates are too low) or removal rates (i.e., NO<sub>y</sub> deposition rates are too slow).

#### 3.4.5 Comparison of OMI NO<sub>2</sub> to Pandora NO<sub>2</sub>

To quantify the skill of the regional OMI NO<sub>2</sub> product, we compare the new total NO<sub>2</sub> vertical columns from the satellite product to the same quantities observed by the Pandora instruments. In Figure 6, monthly averaged

observations during May 2016 from the Pandora instrument are overlaid onto the monthly average of the three OMI NO<sub>2</sub> satellite products. The two regional OMI NO<sub>2</sub> products capture the magnitude and spatial variability of monthly averaged NO<sub>2</sub> within the metropolitan region better.

We then compare daily Pandora observations to each daily OMI NO<sub>2</sub> value spatially and temporally co-located with the Pandora instrument (Figure 6). The Pandora observation is a 2-hour mean centered on the mid-afternoon OMI overpass. The slope of the linear best-fit of the standard product is 0.58, indicating that there is a consistent low bias in the satellite product when the Pandora instrument observes large values. The best-fit slope of the OMI-Regional product with only the air mass factor adjustment (AMF) is 0.76, and the OMI-Regional product with the air mass factor adjustment and spatial kernel (AMF+SK) is 1.07, indicating that the regional products capture the polluted-to-clean spatial gradients best. The correlation of daily observations to the satellite retrievals does not improve between retrievals (OMI-Standard:  $r^2 = 0.57$ , OMI-Regional (AMF):  $r^2 = 0.57$ , and OMI-Regional (AMF+SK):  $r^2 = 0.58$ ). The lack of improvement in the correlation suggests that the forecasted WRF-Chem simulation is unable to capture the daily variability of NO<sub>2</sub> plumes better than a larger scale longer-term average.

### 3.5.6 Estimating NO<sub>x</sub> emissions from Seoul

To estimate NO<sub>x</sub> emissions from the Seoul metropolitan area using a top-down satellite-based approach, we follow the exponentially modified Gaussian (EMG) fitting methodology outlined in Section 2.5. When fit using the EMG method, the photochemical lifetime and OMI NO<sub>2</sub> burden can be derived. Using this information, a NO<sub>x</sub> emission rate can be inferred.

#### 3.5.6.1. Validating the EMG method using WRF-Chem

The WRF-Chem simulation can serve as a test bed to assess the accuracy of the EMG method, since the bottom-up emissions used for the simulation are known. For this study, we find that for Seoul, an across plume width of 160 km encompasses the entire NO<sub>2</sub> downwind plume. Using the NO<sub>2</sub> lifetime, NO<sub>2</sub> burden, and a 160 km across plume width, we calculate the top-down NO<sub>x</sub> emissions rate in the WRF-Chem simulation from the Seoul metropolitan area during the early afternoon (Figure 7). We find the effective NO<sub>2</sub> photochemical lifetime to be  $3.1 \pm 1.3$  hours and the emissions rate to be  $227 \pm 94$  kton/yr NO<sub>2</sub> equivalent. Uncertainties of the top-down NO<sub>x</sub> emissions are the square root of the sum of the squares of: the NO<sub>x</sub> / NO<sub>2</sub> ratio (10%), the OMI NO<sub>2</sub> vertical columns (25%), the across plume width (10%), and the wind fields (30%) (Lu et al., 2015). Only the latter three terms are used to calculate the uncertainty of the NO<sub>2</sub> lifetime (Lu et al., 2015).

The NO<sub>x</sub> bottom-up emissions inventory calculated using a 40 km radius from the Seoul city center is 198 kton/yr NO<sub>2</sub> equivalent. We use a 40 km radius in lieu of a larger radius because an assumption in EMG method is that the emissions must be clustered around a single point (in this case, the city center). Therefore, the calculated emissions rate from the EMG fit is only measuring the magnitude of the perturbing emission source, and not of smaller sources that are further from the city center. Previous studies (de Foy et al., 2014; de Foy et al., 2015) suggest that the

background level calculated by the EMG fit accounts for emissions outside the plume that are more regional and diffuse in nature. The agreement between the top-down (227 kton/yr) and bottom-up (198 kton/yr) approaches demonstrates the accuracy and effectiveness of the EMG method in estimating the emissions rate.

### 3.56.2. Deriving emissions using OMI NO<sub>2</sub>

5 We now calculate the top-down NO<sub>x</sub> emissions rate from the satellite data from the Seoul metropolitan area during the early afternoon (Figure 8). Here we use the OMI standard product and the OMI NO<sub>2</sub> retrieval without the spatial averaging kernel; only the new air mass factor is applied to this retrieval. We do not use the retrieval with the spatial averaging kernel when calculating top-down NO<sub>x</sub> emissions because the spatial averaging is strongly dependent on the wind fields in the WRF-Chem simulation, which are forecasted. Errors in the winds can greatly affect the estimate  
10 using this top-down approach (Valin et al., 2013; de Foy et al., 2014).

For the standard product, the effective NO<sub>2</sub> photochemical lifetime is  $4.2 \pm 1.7$  hours, while in the regional product, the effective lifetime is  $3.4 \pm 1.4$  hours. In the standard product, we derive the NO<sub>x</sub> emissions rate to be  $353 \pm 146$  kton/yr NO<sub>2</sub> equivalent, while in the regional product it is  $484 \pm 201$  kton/yr NO<sub>2</sub> equivalent. Emission estimates using satellite products with coarse resolution air mass factors will yield top-down emission estimates that are lower  
15 than reality. In this case, the regional satellite product yields NO<sub>x</sub> emission rates that are 37% higher; we would expect similar results from other metropolitan regions. The top-down approach for the model simulation yielded a NO<sub>x</sub> emission rate of 227 kton/yr, while the top-down approach using the satellite data yielded a 484 kton/yr NO<sub>x</sub> emission rate: a 53% underestimate in the emissions inventory.

It should be noted that the NO<sub>2</sub> photochemical lifetime derived here is a fundamentally different quantity than the NO<sub>2</sub> lifetime observed by in situ measurements (de Foy et al., 2014; Lu et al., 2015) or derived by model simulations (Lamsal et al., 2010). This is because the lifetime calculation is extremely sensitive to the accuracy of the wind direction (de Foy et al., 2014). Inaccuracies in the wind fields introduce noise that shorten the tail of the fit. As a result, NO<sub>2</sub> photochemical lifetimes derived here are considered “effective” photochemical lifetimes and are universally shorter than the tropospheric column NO<sub>2</sub> lifetimes derived by model simulations (Lamsal et al., 2010). NO<sub>x</sub> sources at the outer portions of urban areas will lead to an artificially longer NO<sub>2</sub> lifetime. This partially compensates for the bias introduced by the wind direction. The effective photochemical lifetime is also different from the NO<sub>2</sub> lifetime derived by in situ measurements of NO<sub>2</sub> at the surface or within the boundary layer. In the boundary layer, NO<sub>2</sub> is consumed faster yielding lifetimes that are shorter than the lifetimes based on tropospheric columns (Nunnermacker et al., 2007).

### 3.67. Model simulation with ~~Double-Increased~~ NO<sub>x</sub> emissions

To test whether an increase doubling in the NO<sub>x</sub> emission rate is appropriate for the Seoul metropolitan area, we conduct a simulation with NO<sub>x</sub> emissions in the Seoul metropolitan area – within a 40 km radius of the city center – increased by a factor of ~~two~~2.13, and analyze the results for May 2016. The 2.13 increase is representative of the

change suggested by the top-down method (OMI-Regional: 484 kton/yr vs. WRF-Chem original: 227 kton/yr). This simulation was performed slightly differently than the original simulation in that it was a continuous month-long simulation and the outer domain was nudged to the reanalysis. We analyzed the results for two days: May 17, 2016 and May 18, 2016. These two days had slow winds speeds and were indicative of days in which local emission sources had a dominating effect on the air quality.

When comparing the new model simulation to in situ observations from the UC-Berkeley NO<sub>2</sub> and NCAR NO<sub>y</sub> instruments aboard the DC-8 aircraft, we find that NO<sub>2</sub> concentrations ~~are~~ isare a bit high, but NO<sub>y</sub> concentrations isare in good agreement with WRF-Chem in the boundary layer when spatially and temporally co-located in the immediate Seoul metropolitan area (Figure 9). When comparing the new WRF-Chem simulation to the OMI-Regional product for May 2016 (Figure 10), we find no significant biases in the Seoul metropolitan area. In the area within 40 km of the Seoul city center, NO<sub>2</sub> columns are now only 11% smaller. ~~This suggests better agreement in NO<sub>2</sub> and NO<sub>y</sub> from a combination of aircraft and satellite data suggests that an increase in NO<sub>x</sub> emissions by a factor of 2.13 is appropriate.~~

Finally, we re-process the air mass factors for May 2016 using the newest WRF-Chem simulation. In Figure 11, we show the OMI-Standard product, the OMI-Regional product with no scaling of the a priori profiles from the original WRF-Chem simulation, the OMI-Regional product with scaling of the original a priori profiles, and the OMI-Regional product with a priori profiles from the new WRF-Chem simulation. While using the new a priori profiles increases the OMI NO<sub>2</sub> retrieval further by 40—208%, this change is much smaller than the 37% changesincrease associated with switching models and model resolution (i.e., Standard vs. Regional product).

#### **4. Conclusions and Discussion**

In this work, we use a high-resolution ( $4 \times 4$  km<sup>2</sup>) WRF-Chem model simulation to re-calculate satellite NO<sub>2</sub> air mass factors over South Korea. We also apply a spatial averaging kernel to better account for the sub-pixel variability that cannot be observed by OMI. The regional OMI NO<sub>2</sub> retrieval yields increased tropospheric columns in city centers and near large industrial areas. In the area within 40 km of the Seoul city center, OMI NO<sub>2</sub> values are 1.37 larger in the regional product. Areas near large industrial sources have OMI NO<sub>2</sub> values that are >2 times larger. The increase in remotely sensed tropospheric vertical column contents in the Seoul metropolitan area is in better agreement with the Pandora NO<sub>2</sub> spectrometer measurements acquired during the KORUS-AQ field campaign.

Using the regional OMI NO<sub>2</sub> product with only the air mass factor correction applied, we derive the NO<sub>x</sub> emissions rate from the Seoul metropolitan area to be  $484 \pm 201$  kton/yr, while the standard NASA OMI NO<sub>2</sub> product gives an emissions rate of  $353 \pm 146$  kton/yr. The WRF-Chem simulation yields a mid-afternoon NO<sub>x</sub> emission rate of  $227 \pm 94$  kton/yr. This suggests an underestimate in the bottom-up NO<sub>x</sub> emissions from Seoul metropolitan area by 53%, when compared to the 484 kton/yr emissions rate from our top-down method. When comparing observed OMI NO<sub>2</sub> to the WRF-Chem model simulation, we find similar underestimates of NO<sub>2</sub> in the Seoul metropolitan area. ~~Interestingly, when comparing NO<sub>2</sub> to aircraft observations, we find that the underestimate exists primarily in the~~

~~Seoul metropolitan area, but not in more rural areas of the country. This suggests that perhaps the NO<sub>x</sub> emission underestimate is primarily confined to the Seoul metropolitan area.~~

The effective photochemical lifetime derived in the Seoul plume is  $4.2 \pm 1.7$  hours using the standard OMI NO<sub>2</sub> product and  $3.4 \pm 1.4$  hours using the regional product. The regional product yields shorter NO<sub>2</sub> lifetimes, although it is not a statistically significant difference. ~~It should be noted that the NO<sub>2</sub> photochemical lifetime derived here is a fundamentally different quantity than the NO<sub>2</sub> lifetime observed by in situ measurements (de Foy et al., 2014; Lu et al., 2015) or derived by model simulations (Lamsal et al., 2010). This is because the lifetime calculation is extremely sensitive to the accuracy of the wind direction. Inaccuracies in the wind fields introduce noise that shorten the tail of the fit. As a result, NO<sub>2</sub> photochemical lifetimes derived here are considered “effective” photochemical lifetimes and are universally shorter than the tropospheric column NO<sub>2</sub> lifetimes derived by model simulations (Lamsal et al., 2010). The effective photochemical lifetime is also different than a NO<sub>2</sub> lifetime derived by in situ measurements observing NO<sub>2</sub> at the surface or within the boundary layer: boundary layer where NO<sub>2</sub> is consumed faster yielding lifetimes that are shorter compared to the tropospheric column lifetimes (Nunnermacker et al., 2007). Finally, we show that a WRF-Chem simulation with an increase in the NO<sub>x</sub> emissions by a factor of 2.13 yields a better comparison with aircraft observations of NO<sub>2</sub> and NO<sub>y</sub>, and is in better agreement with the OMI-Regional NO<sub>2</sub> product developed herein.~~

It should be noted that the Seoul metropolitan area has complex geographical features, which adds further uncertainty to this analysis. The area has large topographical changes over short distances, including many hills (> 500 m) within the metropolitan area. Furthermore, the city is in close proximity to the Yellow Sea, which causes the area to be affected by sea breeze fronts, especially in the springtime, which is our period of focus. The localized mountain and sea breezes may not be fully captured by our 4 × 4 km<sup>2</sup> WRF-Chem simulation used to derive the OMI-Regional product or the ERA-interim dataset used to calculate top-down NO<sub>x</sub> emissions. The effects of these features on local air quality have been documented elsewhere in the literature (Kim and Ghim, 2002; Lee et al., 2008; Ryu et al., 2013). We do not expect any consistent bias to result from this added uncertainty. Nevertheless, the 4 × 4 km<sup>2</sup> simulation will capture topography and mesoscale phenomena better than a coarse global model and further supports the benefits of WRF-Chem over a global model to derive NO<sub>2</sub> vertical column contents.

We ~~demonstrate~~ hypothesize that the temporalization of NO<sub>x</sub> emissions in the bottom-up emission inventory is a large remaining uncertainty. The satellite-derived emission rates are instantaneous rates at the time of the OMI overpass (~13:45 local time). This is a different quantity than a bottom-up NO<sub>x</sub> emission inventory, which is often a daily averaged or monthly averaged emission rate. For this study, we only attempt to derive a mid-afternoon NO<sub>x</sub> emission rate. Subsequently, we make sure to compare this to the mid-afternoon NO<sub>x</sub> emission rate from WRF-eChem. While bottom-up studies provide estimates of the diurnal variability of NO<sub>x</sub> emissions, these are very difficult to confirm from top-down approaches. Due to a consistent mid-afternoon overpass time, OMI or TROPOMI cannot address this issue. Due to boundary layer dynamics, this is also very difficult to constrain from ground-based and aircraft measurements. In the future, observations from a geostationary satellite instruments such as the Geostationary

Environment Monitoring Spectrometer (GEMS) and Tropospheric Emissions: Monitoring Pollution (TEMPO), will be helpful in constraining the ratio of the mid-afternoon emissions rate to the 24-hour averaged emission rate.

## Acknowledgments

This publication was developed using funding from the NASA KORUS-AQ science team and the NASA Atmospheric Composition Modeling and Analysis Program (ACMAP). We would like to thank the NASA Pandora Project Team, including Jay Herman and Bob Swap of NASA Goddard Space Flight Center, Jim Szykman of EPA, and the ESA-Pandonia team from Luftblick in supporting the deployment and maintenance of the Pandora instruments as well as the acquisition and processing of those observations during KORUS-AQ. We would also like to thank Ron Cohen of UC-Berkeley and his research group for their observations of NO<sub>2</sub> from the DC-8 aircraft during this same time period, and Andy Weinheimer of NCAR and his research group for their observations of NO<sub>y</sub> from the DC-8 aircraft. We would also like to thank Louisa Emmons and Gaby Pfister for their support in running the WRF-Chem simulation.

10 Additionally, we would like to thank Jim Crawford of NASA Langley and Barry Lefter of NASA Headquarters for their input on this research article. All data from KORUS-AQ can be downloaded freely from <http://www-air.larc.nasa.gov/cgi-bin/ArcView/discover-aq.dc-2011>. We acknowledge the free use of NO<sub>2</sub> column data from the OMI sensor available at: [https://disc.gsfc.nasa.gov/Aura/data-holdings/OMI/omno2\\_v003.shtml](https://disc.gsfc.nasa.gov/Aura/data-holdings/OMI/omno2_v003.shtml). The submitted manuscript has been created by UChicago Argonne, LLC, Operator of Argonne National Laboratory (“Argonne”).

15 Argonne, a U.S. Department of Energy Office of Science laboratory, is operated under Contract No. DE-AC02-06CH11357. The U.S. Government retains for itself, and others acting on its behalf, a paid-up nonexclusive, irrevocable worldwide license in said article to reproduce, prepare derivative works, distribute copies to the public, and perform publicly and display publicly, by or on behalf of the Government.

## References

- Allen, D. J., Pickering, K. E., Pinder, R. W., Henderson, B. H., Appel, K. W., and Prados, A.: Impact of lightning-NO on eastern United States photochemistry during the summer of 2006 as determined using the CMAQ model, *Atmos. Chem. Phys.*, 12, 1737-1758, 2012.
- 5 Beirle, S., Boersma, K. F., Platt, U., Lawrence, M. G., and Wagner, T.: Megacity Emissions and Lifetimes of Nitrogen Oxides Probed from Space, *Science*, 333, 1737-1739, 2011.
- Boersma, K. F., Jacob, D. J., Bucsela, E. J., Perring, A. E., Dirksen, R., Yantosca, R. M., Park, R. J., Wenig, M. O., Bertram, T. H., and Cohen, R. C.: Validation of OMI tropospheric NO<sub>2</sub> observations during INTEX-B and application to constrain NO<sub>x</sub> emissions over the eastern United States and Mexico, *Atmos. Environ.*, 42, 4480-4497, 2008.
- 10 Boersma, K. F., Eskes, H. J., Dirksen, R. J., Veefkind, J. P., Stammes, P., Huijnen, V., Kleipool, Q. L., Sneep, M., Claas, J., and Leitão, J.: An improved tropospheric NO<sub>2</sub> column retrieval algorithm for the Ozone Monitoring Instrument, *Atmos. Meas. Tech.*, 4, 1905, 2011.
- Boersma, K. F., Vinken, G. C. M., and Tournadre, J.: Ships going slow in reducing their NO<sub>x</sub> emissions: changes in 2005–2012 ship exhaust inferred from satellite measurements over Europe, *Environ. Res. Lett.*, 10, 074007, 2015.
- 15 Bucsela, E., Krotkov, N., Celarier, E., Lamsal, L., Swartz, W., Bhartia, P., Boersma, K., Veefkind, J., Gleason, J., and Pickering, K.: A new algorithm for retrieving vertical column NO<sub>2</sub> from nadir-viewing satellite instruments: applications to OMI, *Atmos. Meas. Tech.*, 6, 1361-1407, 2013.
- [Burrows, J. P., Weber, M., Buchwitz, M., Rozanov, V., Ladstätter, M., Weissenmayer, A., Richter, A., DeBeek, R., Hoogen, R., Bramstedt, K., Eichmann, K.-U., Eisinger, M., and Perner, D.: The Global Ozone Monitoring Experiment \(GOME\): Mission Concept and First Scientific Results, \*J. Atmos. Sci.\*, 56, 151–175, 1999.](#)
- 20 Canty, T. P., Hembeck, L., Vinciguerra, T. P., Anderson, D. C., Goldberg, D. L., Carpenter, S. F., Allen, D. J., Loughner, C. P., Salawitch, R. J., and Dickerson, R. R.: Ozone and NO<sub>x</sub> chemistry in the eastern US: evaluation of CMAQ/CB05 with satellite (OMI) data, *Atmos. Chem. Phys.*, 15, 10965-10982, 2015.
- 25 Chen, D., Zhou, B., Beirle, S., Chen, L. M., and Wagner, T.: Tropospheric NO<sub>2</sub> column densities deduced from zenith-sky DOAS measurements in Shanghai, China, and their application to satellite validation, *Atmos. Chem. Phys.*, 9, 3641-3662, 2009.
- Curier, R. L., Kranenburg, R., Segers, A. J. S., Timmermans, R. M. A., and Schaap, M.: Synergistic use of OMI NO<sub>2</sub> tropospheric columns and LOTOS-EUROS to evaluate the NO<sub>x</sub> emission trends across Europe, *Remote Sensing of Environment*, 149, 58-69, 2014.
- 30 Day, D. A., Wooldridge, P. J., Dillon, M. B., Thornton, J. A., and Cohen, R. C.: A thermal dissociation laser-induced fluorescence instrument for in situ detection of NO<sub>2</sub>, peroxy nitrates, alkyl nitrates, and HNO<sub>3</sub>, *J. Geophys. Res. Atmos.*, 107, ARTN 4046, 2002.
- Dee, D. P., Uppala, S. M., Simmons, A. J., Berrisford, P., Poli, P., Kobayashi, S., Andrae, U., Balmaseda, M. A., Balsamo, G., Bauer, P., Bechtold, P., Beljaars, A. C. M., van de Berg, L., Bidlot, J., Bormann, N., Delsol, C., Dragani, R., Fuentes, M., Geer, A. J., Haimberger, L., Healy, S. B., Hersbach, H., Hólm, E. V., Isaksen, I., Kållberg, P., Köhler, M., Matricardi, M., McNally, A. P., Monge-Sanz, B. M., Morcrette, J.-J., Park, B.-K., Peubey, C., de Rosnay, P., Tavolato, C., Thépaut, J.-N., and Vitart, F.: The ERA-Interim reanalysis: configuration and performance of the data assimilation system, *Q. J. Roy. Meteorol. Soc.*, 137, 553– 597, doi:10.1002/qj.828, 2011.
- 40 de Foy, B., Lu, Z., and Streets, D. G.: Satellite NO<sub>2</sub> retrievals suggest China has exceeded its NO<sub>x</sub> reduction goals from the twelfth Five-Year Plan, *Scientific Reports*, 6, 2016.
- de Foy, B., Lu, Z., Streets, D. G., Lamsal, L. N., and Duncan, B. N.: Estimates of power plant NO<sub>x</sub> emissions and lifetimes from OMI NO<sub>2</sub> satellite retrievals, *Atmos. Environ.*, 116, 1-11, 2015.
- 45 de Foy, B., Wilkins, J. L., Lu, Z., Streets, D. G., Duncan, B. N.: Model evaluation of methods for estimating surface emissions and chemical lifetimes from satellite data. *Atmos. Environ.* 98, 66-77, 2014.
- Dobber, M., Kleipool, Q., Dirksen, E., Levelt, P., Jaross, G., Taylor, S., Kelly, T., Flynn, L., Leppelmeier, G., and Rozemeijer, N.: Validation of Ozone Monitoring Instrument level 1b data products, *J. Geophys. Res. Atmos.*, 113, D15S06, 2008.
- 50 Duncan, B. N., Lamsal, L. N., Thompson, A. M., Yoshida, Y., Lu, Z., Streets, D. G., Hurwitz, M. M., and Pickering, K. E.: A space based, high resolution view of notable changes in urban NO<sub>x</sub> pollution around the world (2005–2014), *J. Geophys. Res. Atmos.*, 121, 976-996, 2016.
- Flynn, C. M., Pickering, K. E., Crawford, J. H., Lamsal, L., Krotkov, N., Herman, J., Weinheimer, A., Chen, G., Liu, X., and Szykman, J.: Relationship between column-density and surface mixing ratio: Statistical analysis of O<sub>3</sub>

- and NO<sub>2</sub> data from the July 2011 Maryland DISCOVER-AQ mission, *Atmos. Environ.*, 92, 429-441, 2014.
- Goldberg, D. L., Lamsal, L. N., Loughner, C. P., Swartz, W. H., Lu, Z., and Streets, D. G.: A high-resolution and observationally constrained OMI NO<sub>2</sub> satellite retrieval, *Atmos. Chem. Phys.*, 17, 11403-11421, <https://doi.org/10.5194/acp-17-11403-2017>, 2017.
- 5 Goldberg, D. L., Vinciguerra, T. P., Anderson, D. C., Hembeck, L., Canty, T. P., Ehrman, S. H., Martins, D. K., Stauffer, R. M., Thompson, A. M., Salawitch, R. J., and Dickerson R. R.: CAMx ozone source attribution in the eastern United States using guidance from observations during DISCOVER-AQ Maryland, *Geophys. Res. Lett.*, 43, <https://dx.doi.org/10.1002/2015GL067332>, 2016.
- 10 Grell, G., Peckham, S. E., Schmitz, R., McKeen, S. A., Frost, G., Skamarock, W. C., and Eder, B.: Fully coupled “online” chemistry within the WRF model, *Atmospheric Environment*, 39, 6957-6975, [10.1016/j.atmosenv.2005.04.027](https://doi.org/10.1016/j.atmosenv.2005.04.027), 2005.
- Han, K. M., Lee, S., Chang, L. S., and Song, C. H.: A comparison study between CMAQ-simulated and OMI-retrieved NO<sub>2</sub> columns over East Asia for evaluation of NO<sub>x</sub> emission fluxes of INTEX-B, CAPSS, and REAS inventories, *Atmos. Chem. Phys.*, 15, 1913-1938, 2015.
- 15 Herman, J., Cede, A., Spinei, E., Mount, G., Tzortziou, M., and Abuhassan, N.: NO<sub>2</sub> column amounts from ground-based Pandora and MFDOAS spectrometers using the direct-sun DOAS technique: Intercomparisons and application to OMI validation, *J. Geophys. Res.*, 114, D13307, 2009.
- Herman, J., Spinei, E., Fried, A., Kim, J., Kim, J., Kim, W., Cede, A., Abuhassan, N., and Segal-Rozenhaimer, M.: NO<sub>2</sub> and HCHO measurements in Korea from 2012 to 2016 from Pandora spectrometer instruments compared with OMI retrievals and with aircraft measurements during the KORUS-AQ campaign, *Atmos. Meas. Tech.*, 11, 4583-4603, <https://doi.org/10.5194/amt-11-4583-2018>, 2018
- 20 Hilboll, A., Richter, A., and Burrows, J. P.: Long-term changes of tropospheric NO<sub>2</sub> over megacities derived from multiple satellite instruments, *Atmos. Chem. Phys.*, 13, 4145-4169, 2013.
- Hodzic, A., and Jimenez, J. L.: Modeling anthropogenically controlled secondary organic aerosols in a megacity: a simplified framework for global and climate models, *Geosci. Model Dev.*, 4, 901-917, [10.5194/gmd-4-901-2011](https://doi.org/10.5194/gmd-4-901-2011), 2011.
- 25 Hudman, R. C., Russell, A. R., Valin, L. C., and Cohen, R. C.: Interannual variability in soil nitric oxide emissions over the United States as viewed from space, *Atmos. Chem. Phys.*, 10, 9943-9952, 2010.
- Huijnen, V., Eskes, H. J., Poupkou, A., Elbern, H., Boersma, K. F., Foret, G., Sofiev, M., Valdebenito, A., Flemming, J., Stein, O., Gross, A., Robertson, L., D’Isidoro, M., Kioutsioukis, I., Friese, E., Amstrup, B., Bergstrom, R., Strunk, A., Vira, J., Zyryanov, D., Maurizi, A., Melas, D., Peuch, V.-H., and Zerefos, C.: Comparison of OMI NO<sub>2</sub> tropospheric columns with an ensemble of global and European regional air quality models, *Atmos. Chem. Phys.*, 10, 3273-3296, [doi:10.5194/acp-10-3273-2010](https://doi.org/10.5194/acp-10-3273-2010), 2010.
- 30 Ialongo, I., Herman, J., Krotkov, N., Lamsal, L., Boersma, K. F., Hovila, J., and Tamminen, J.: Comparison of OMI NO<sub>2</sub> observations and their seasonal and weekly cycles with ground-based measurements in Helsinki, *Atmos. Meas. Tech.*, 9, 5203, 2016.
- Inness, A., Blechschmidt, A. M., Bouarar, I., Chabrilat, S., Crepulja, M., Engelen, R. J., Eskes, H., Flemming, J., Gaudel, A., Hendrick, F., Huijnen, V., Jones, L., Kapsomenakis, J., Katragkou, E., Keppens, A., Langerock, B., de Mazière, M., Melas, D., Parrington, M., Peuch, V. H., Razinger, M., Richter, A., Schultz, M. G., Suttie, M., Thouret, V., Vrekoussis, M., Wagner, A., and Zerefos, C.: Data assimilation of satellite retrieved ozone, carbon monoxide and nitrogen dioxide with ECMWF’s Composition-IFS, *Atmos. Chem. Phys. Discuss.*, 15, 4265-4331, [10.5194/acpd-15-4265-2015](https://doi.org/10.5194/acpd-15-4265-2015), 2015.
- Kim, H. C., Lee, P., Judd, L., Pan, L., and Lefer, B.: OMI NO<sub>2</sub> column densities over North American urban cities: the effect of satellite footprint resolution, *Geosci. Mod. Dev.*, 9, 1111-1123, 2016.
- 45 Kim, J. Y., and Ghim, Y. S.: Effects of the density of meteorological observations on the diagnostic wind fields and performance of photochemical modeling in the great Seoul area, *Atmos. Environ.*, 36, 201-212, 2002.
- Kleipool, Q. L., Dobber, M. R., de Haan, J. F., and Levelt, P. F.: Earth surface reflectance climatology from 3 years of OMI data, *J. Geophys. Res. Atmos.*, 113, 2008.
- 50 Krotkov, N. A., McLinden, C. A., Li, C., Lamsal, L. N., Celarier, E. A., Marchenko, S. V., Swartz, W. H., Bucsela, E. J., Joiner, J., and Duncan, B. N.: Aura OMI observations of regional SO<sub>2</sub> and NO<sub>2</sub> pollution changes from 2005 to 2014, *Atmos. Chem. Phys.*, 16, 4605-4629, 2016.
- Krotkov, N. A., Lamsal, L. N., Celarier, E. A., Swartz, W. H., Marchenko, S. V., Bucsela, E. J., Chan, K. L., and Wenig, M. O.: The version 3 OMI NO<sub>2</sub> standard product, *Atmos. Meas. Tech. Discuss.*, in review, 2017.
- 55 Kuhlmann, G., Lam, Y. F., Cheung, H. M., Hartl, A., Fung, J. C. H., Chan, P. W., and Wenig, W. O.: Development of a custom OMI NO<sub>2</sub> data product for evaluating biases in a regional chemistry transport model, *Atmos. Chem. Phys.*, 15, 5627-5644, 2015.

- Lamsal, L. N., Martin, R. V., van Donkelaar, A., Steinbacher, M., Celarier, E. A., Bucsela, E., Dunlea, E. J., and Pinto, J. P.: Ground-level nitrogen dioxide concentrations inferred from the satellite-borne Ozone Monitoring Instrument, *J. Geophys. Res.*, 113, D16308, 2008.
- 5 [Lamsal, L. N., Martin, R. V., van Donkelaar, A., Celarier, E. A., Bucsela, E. J., Boersma, K. F., Dirksen, R., Luo, C., and Wang, Y.: Indirect validation of tropospheric nitrogen dioxide retrieved from the OMI satellite instrument: Insight into the seasonal variation of nitrogen oxides at northern midlatitudes, \*J. Geophys. Res.\*, 115, D05302, doi:10.1029/2009jd013351, 2010.](#)
- Lamsal, L. N., Krotkov, N. A., Celarier, E. A., Swartz, W. H., Pickering, K. E., Bucsela, E. J., Gleason, J. F., Martin, R. V., Philip, S., and Irie, H.: Evaluation of OMI operational standard NO<sub>2</sub> column retrievals using in situ and surface-based NO<sub>2</sub> observations, *Atmos. Chem. Phys.*, 14, 11587-11609, 2014.
- 10 Lamsal, L. N., Duncan, B. N., Yoshida, Y., Krotkov, N. A., Pickering, K. E., Streets, D. G., and Lu, Z.: US NO<sub>2</sub> trends (2005 - 2013): EPA Air Quality System (AQS) data versus improved observations from the Ozone Monitoring Instrument (OMI), *Atmos. Environ.*, 110, 130-143, 2015.
- Laughner, J. L., Zare, A., and Cohen, R. C.: Effects of daily meteorology on the interpretation of space-based remote sensing of NO<sub>2</sub>, *Atmos. Chem. Phys.*, 16, 15247-15264, 2016.
- 15 [Lee, H. W., Choi, H.-J., Lee, S.-H., Kim, Y.-K., Jung, W.-S.: The impact of topography and urban building parameterization on the photochemical ozone concentration of Seoul, Korea, \*Atmos. Environ.\*, 42\(18\), 4232-4246, 2008.](#)
- Levelt, P. F., Van den Oord, G. H. J., Dobber, M. R., Malkki, A., Visser, H., de Vries, J., Stammes, P., Lundell, J. O. V., and Saari, H.: The Ozone Monitoring Instrument, *IEEE Trans. Geosci. Rem. Sens.*, 44, 1093-1101, 2006.
- 20 Liaskos, C. E., Allen, D. J., and Pickering, K. E.: Sensitivity of tropical tropospheric composition to lightning NO<sub>x</sub> production as determined by replay simulations with GEOS-5, *J. Geophys. Res. Atmos.*, 2015.
- Lin, J. T., Liu, M. Y., Xin, J. Y., Boersma, K. F., Spurr, R., Martin, R., and Zhang, Q.: Influence of aerosols and surface reflectance on satellite NO<sub>2</sub> retrieval: seasonal and spatial characteristics and implications for NO<sub>x</sub> emission constraints, *Atmos. Chem. Phys.*, 15, 11217-11241, 2015.
- 25 Liu, F., Beirle, S., Zhang, Q., Dörner, S., He, K., and Wagner, T.: NO<sub>x</sub> lifetimes and emissions of cities and power plants in polluted background estimated by satellite observations, *Atmos. Chem. Phys.*, 16, 5283-5298, <https://doi.org/10.5194/acp-16-5283-2016>, 2016.
- Liu, F., Beirle, S., Zhang, Q., van der A, R. J., Zheng, B., Tong, D., and He, K.: NO<sub>x</sub> emission trends over Chinese cities estimated from OMI observations during 2005 to 2015, *Atmos. Chem. Phys.*, 17, 9261-9275, <https://doi.org/10.5194/acp-17-9261-2017>, 2017.
- 30 Lorente, A., Boersma, K. F., Yu, H., Dörner, S., Hilboll, A., Richter, A., Liu, M., Lamsal, L. N., Barkley, M., and De Smedt, I.: Structural uncertainty in air mass factor calculation for NO<sub>2</sub> and HCHO satellite retrievals, *Atmos. Meas. Tech.*, 10, 759, 2017.
- 35 Lu, Z., Streets, D. G., de Foy, B., Lamsal, L. N., Duncan, B. N., and Xing, J.: Emissions of nitrogen oxides from US urban areas: estimation from Ozone Monitoring Instrument retrievals for 2005–2014, *Atmos. Chem. Phys.*, 15, 10367-10383, 2015.
- Ma, J. Z., Beirle, S., Jin, J. L., Shaiganfar, R., Yan, P., and Wagner, T.: Tropospheric NO<sub>2</sub> vertical column densities over Beijing: results of the first three years of ground-based MAX-DOAS measurements (2008–2011) and satellite validation, *Atmos. Chem. Phys.*, 13, 1547-1567, 2013.
- 40 Martin, R. V., Chance, K., Jacob, D. J., Kurosu, T. P., Spurr, R. J. D., Bucsela, E., Gleason, J. F., Palmer, P. I., Bey, I., and Fiore, A. M.: An improved retrieval of tropospheric nitrogen dioxide from GOME, *J. Geophys. Res. Atmos.*, 107, 2002.
- 45 [Miyazaki, K., Eskes, H., Sudo, K., Boersma, K. F., Bowman, K., and Kanaya, Y.: Decadal changes in global surface NO<sub>x</sub> emissions from multi-constituent satellite data assimilation, \*Atmos. Chem. Phys.\*, 17, 807-837, <https://doi.org/10.5194/acp-17-807-2017>, 2017.](#)
- Nault, B. A., Laughner, J. L., Wooldridge, P. J., Crouse, J. D., Dibb, J., Diskin, G., Peischl, J., Podolske, J. R., Pollack, I. B., Ryerson, T. B., Scheuer, E., Wennberg, P. O., and Cohen, R. C.: Lightning NO<sub>x</sub> Emissions: Reconciling Measured and Modeled Estimates With Updated NO<sub>x</sub> Chemistry, *Geophys. Res. Lett.*, 44, 9479–9488, <https://doi.org/10.1002/2017GL074436>, 2017.
- 50 Palmer, P. I., Jacob, D. J., Chance, K. V., Martin, R. V., Spurr, R. J. D., Kurosu, T., Bey, I., Yantosca, R. M., Fiore, A., and Li, Q.: Air mass factor formulation for spectroscopic measurements from satellites: Application to formaldehyde retrievals from the Global Ozone Monitoring Experiment, *J. Geophys. Res.*, 106, 14539-14550, 2001.
- 55 Pfister, G. G., Walters, S., Lamarque, J. F., Fast, J., Barth, M. C., Wong, J., Done, J., Holland, G., and Bruyère, C. L.: Projections of future summertime ozone over the U.S, *Journal of Geophysical Research: Atmospheres*, 119, 5559-

- 5582, 10.1002/2013jd020932, 2014.
- Pickering, K. E., Bucsel, E., D. Ring, A., Holzworth, R., and Krotkov, N.: Estimates of lightning NO<sub>x</sub> production based on OMI NO<sub>2</sub> observations over the Gulf of Mexico, *J. Geophys. Res. Atmos.*, 121, 8668-8691, 2016.
- 5 Platt, U.: Differential optical absorption spectroscopy (DOAS), *Air monitoring by spectroscopic technique*, 127, 27-84, 1994.
- Pujadas, M., Núñez, L., and Lubrani, P.: Assessment of NO<sub>2</sub> satellite observations for en-route aircraft emissions detection, *Remote Sensing of Environment*, 115, 3298-3312, 2011.
- Rasool, Q. Z., Zhang, R., Lash, B., and Cohan, D. S., Cooter, E. J., Bash, J. O., Lamsal, L. N.: Enhanced representation of soil NO emissions in the Community Multiscale Air Quality (CMAQ) model version 5.0. 2, *Geosci. Mod. Dev.*, 9, 3177-3197, 2016.
- 10 [Ridley, B., Ott, L., Pickering, K., Emmons, L., Montzka, D., Weinheimer, A., Knapp, D., Grahek, F., Li, L., Heymsfield, G., McGill, M., Kucera, P., Mahoney, M. J., Baumgarner, D., Schultz, M., and Brasseur, G.: Florida thunderstorms: A faucet of reactive nitrogen to the upper troposphere, \*J. Geophys. Res. Atmos.\*, 109, D17305, 2004.](#)
- 15 [Romer, P. S., Duffey, K. C., Wooldridge, P. J., Allen, H. M., Ayres, B. R., Brown, S. S., Brune, W. H., Crouse, J. D., de Gouw, J., Draper, D. C., Feiner, P. A., Fry, J. L., Goldstein, A. H., Koss, A., Miszta, P. K., Nguyen, T. B., Olson, K., Teng, A. P., Wennberg, P. O., Wild, R. J., Zhang, L., and Cohen, R. C.: The lifetime of nitrogen oxides in an isoprene-dominated forest, \*Atmos. Chem. Phys.\*, 16, 7623-7637, <https://doi.org/10.5194/acp-16-7623-2016>, 2016.](#)
- 20 Russell, A. R., Valin, L. C., Bucsel, E. J., Wenig, M. O., and Cohen, R. C.: Space-based constraints on spatial and temporal patterns of NO<sub>x</sub> emissions in California, 2005-2008, *Environ. Sci. Technol.*, 44, 3608-3615, 2010.
- Russell, A. R., Perring, A. E., Valin, L. C., Bucsel, E. J., Browne, E. C., Wooldridge, P. J., and Cohen, R. C.: A high spatial resolution retrieval of NO<sub>2</sub> column densities from OMI: method and evaluation, *Atmos. Chem. Phys.*, 11, 8543-8554, 2011.
- 25 [Ryu, Y.-H., Baik, J.-J., Kwak, K.-H., Kim, S., and Moon, N.: Impacts of urban land-surface forcing on ozone air quality in the Seoul metropolitan area, \*Atmos. Chem. Phys.\*, 13, 2177-2194, <https://doi.org/10.5194/acp-13-2177-2013>, 2013.](#)
- 30 Saide, P. E., Carmichael, G. R., Liu, Z., Schwartz, C. S., Lin, H. C., da Silva, A. M., and Hyer, E.: Aerosol optical depth assimilation for a size-resolved sectional model: impacts of observationally constrained, multi-wavelength and fine mode retrievals on regional scale forecasts, *Atmos. Chem. Phys. Discuss.*, 13, 12213-12261, 10.5194/acpd-13-12213-2013, 2013.
- Saide, P. E., Kim, J., Song, C. H., Choi, M., Cheng, Y., and Carmichael, G. R.: Assimilation of next generation geostationary aerosol optical depth retrievals to improve air quality simulations, *Geophysical research letters*, 41, 2014GL062089, 10.1002/2014gl062089, 2014.
- 35 Skamarock, W. C., Klemp, J. B., Dudhia, J., Gill, D. O., Barker, D. M., Duda, M. G., Huang, X.-Y., Wang, W., and Powers, J. G.: A description of the Advanced Research WRF version 3, NCAR Tech. Note NCAR/TN-475+ STR, 2008.
- Souri, A. H., Choi, Y., Jeon, W., Li, X., Pan, S., Diao, L., and Westenbarger, D. A.: Constraining NO<sub>x</sub> emissions using satellite NO<sub>2</sub> measurements during 2013 DISCOVER-AQ Texas campaign, *Atmos. Environ.*, 131, 371-381, 2016.
- 40 Souri, A. H., Choi, Y., Jeon, W., Woo, J., Zhang, Q., and Kurokawa, J.: Remote sensing evidence of decadal changes in major tropospheric ozone precursors over East Asia *J. Geophys. Res. Atmos.*, 2017.
- 45 Streets, D. G., Carty, T., Carmichael, G. R., de Foy, B., Dickerson, R. R., Duncan, B. N., Edwards, D. P., Haynes, J. A., Henze, D. K., Houyoux, M. R., Jacob, D. J., Krotkov, N. A., Lamsal, L. N., Liu, Y., Lu, Z., Martin, R. V., Pfister, G. G., Pinder, R. W., Salawitch, R. J., Wecht, K. J.: Emissions estimation from satellite retrievals: A review of current capability, *Atmos. Environ.*, 77, 1011-1042, 2013.
- Thornton, J. A., Wooldridge, P. J., and Cohen R. C.: Atmospheric NO<sub>2</sub>: In situ laser-induced fluorescence detection at parts per trillion mixing ratios, *Analytical Chemistry*, 72, 528-539, 2000.
- 50 Valin, L. C., Russell, A. R., and Cohen, R. C.: Variations of OH radicals in an urban plume inferred from NO<sub>2</sub> column measurements. *Geophys. Res. Lett.*, 40, 1856-1860, 2013.
- van der A, R. J., Mijling, B., Ding, J., Koukouli, M. E., Liu, F., Li, Q., Mao, H., Theys, N.: Cleaning up the air: effectiveness of air quality policy for SO<sub>2</sub> and NO<sub>x</sub> emissions in China, *Atmos. Chem. Phys.*, 17, 1775-1789, 2017.
- 55 van Vuuren, D. P., Bouwman, L. F., Smith, S. J., and Dentener, F.: Global projections for anthropogenic reactive nitrogen emissions to the atmosphere: an assessment of scenarios in the scientific literature, *Current Opinion in*

Environmental Sustainability, 3, 359-369, 2011.

Vandaele, A. C., Hermans, C., Simon, P. C., Carleer, M., Colin, R., Fally, S., Merienne, M.-F., Jenouvrier, A., and Coquart, B.: Measurements of the NO<sub>2</sub> absorption cross-section from 42 000 cm<sup>-1</sup> to 10 000 cm<sup>-1</sup> (238–1000 nm) at 220 K and 294 K, *Journal of Quantitative Spectroscopy and Radiative Transfer*, 59, 171-184, 1998.

5 Vasilkov, A., Qin, W., Krotkov, N., Lamsal, L., Spurr, R., Haffner, D., Joiner, J., Yang, E.-S., and Marchenko, S.: Accounting for the effects of surface BRDF on satellite cloud and trace-gas retrievals: a new approach based on geometry-dependent Lambertian equivalent reflectivity applied to OMI algorithms, *Atmos. Meas. Tech.*, 10, 333-349, <https://doi.org/10.5194/amt-10-333-2017>, 2017.

10 Vinken, G. C. M., Boersma, K. F., Maasakkers, J. D., Adon, M., and Martin, R. V.: Worldwide biogenic soil NO<sub>x</sub> emissions inferred from OMI NO<sub>2</sub> observations, *Atmos. Chem. Phys.*, 14, 10363-10381, 2014a.

Vinken, G. C. M., Boersma, K. F., van Donkelaar, A., and Zhang, L.: Constraints on ship NO<sub>x</sub> emissions in Europe using GEOS-Chem and OMI satellite NO<sub>2</sub> observations, *Atmos. Chem. Phys.*, 14, 1353-1369, 2014b.

15 Woo, J. H., Choi, K. C., Kim, H. K., Baek, B. H., Jang, M., Eum, J. H., Song, C. H., Ma, Y. I., Sunwoo, Y., Chang, L. S., and Yoo, S. H.: Development of an anthropogenic emissions processing system for Asia using SMOKE, *Atmos. Environ.*, 58, 5–13, 2012.

Zaveri, R. A., Easter, R. C., Fast, J. D., and Peters, L. K.: Model for simulating aerosol interactions and chemistry (MOSAIC), *J. Geophys. Res.*, 113, D13204, 2008.

20 Zhang, L., Jacob, D. J., Boersma, K. F., Jaffe, D. A., Olson, J. R., Bowman, K. W., Worden, J. R., Thompson, A. M., Avery, M. A., Cohen, R. C., Dibb, J. E., Flock, F. M., Fuelberg, H. E., Huey, L. G., McMillan, W. W., Singh, H. B., and Weinheimer, A. J.: Transpacific transport of ozone pollution and the effect of recent Asian emission increases on air quality in North America: an integrated analysis using satellite, aircraft, ozonesonde, and surface observations, *Atmos. Chem. Phys.*, 8, 6117-6136, 2008.

25 Zheng, B., Tong, D., Li, M., Liu, F., Hong, C., Geng, G., Li, H., Li, X., Peng, L., Qi, J., Yan, L., Zhang, Y., Zhao, H., Zheng, Y., He, K., and Zhang, Q.: Trends in China's anthropogenic emissions since 2010 as the consequence of clean air actions, *Atmos. Chem. Phys.*, 18, 14095-14111, <https://doi.org/10.5194/acp-18-14095-2018>, 2018.

Zhou, Y., Brunner, D., Spurr, R. J. D., Boersma, K. F., Sneep, M., Popp, C., and Buchmann, B.: Accounting for surface reflectance anisotropy in satellite retrievals of tropospheric NO<sub>2</sub>, *Atmos. Meas. Tech.*, 3, 1185-1203, <https://doi.org/10.5194/amt-3-1185-2010>, 2010.

30 Zhou, Y., Brunner, D., Boersma, K. F., Dirksen, R., and Wang, P.: An improved tropospheric NO<sub>2</sub> retrieval for OMI observations in the vicinity of mountainous terrain, *Atmos. Meas. Tech.*, 2, 401-416, <https://doi.org/10.5194/amt-2-401-2009>, 2009.

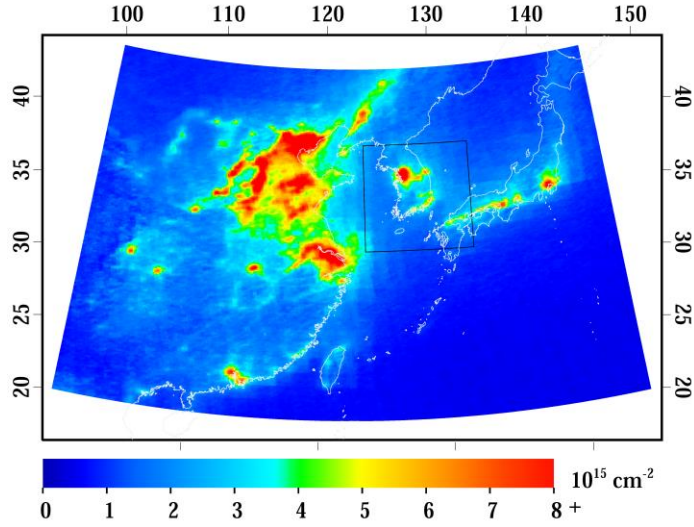


**Figure 1.** Warm season averaged (May – Sept) NO<sub>2</sub> tropospheric vertical column content using the standard-OMI-Standard NO<sub>2</sub> product for the years of 2015 – 2017 in (a) the United States and (b) East Asia. The 4 × 4 km<sup>2</sup> WRF-Chem domain is outlined over the Korean peninsula.

5

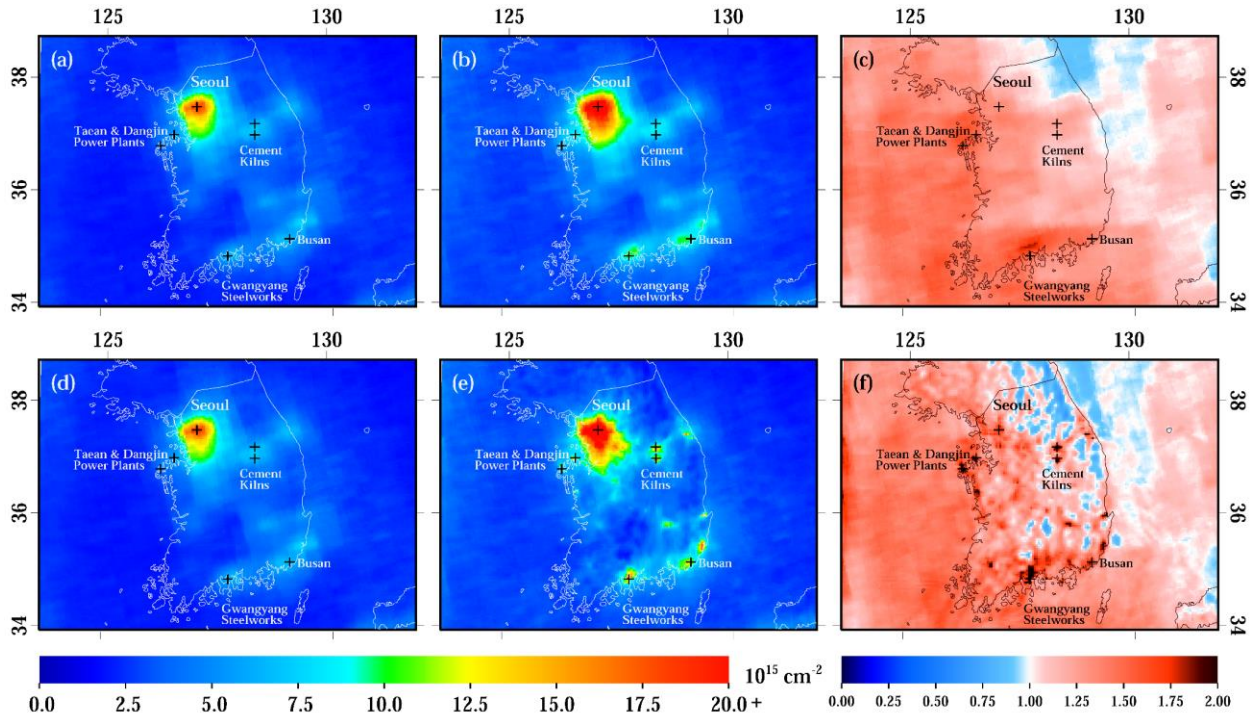


**Figure 2.** (a) OMI-Standard NO<sub>2</sub> product averaged over a 9-month period, Apr – Jun 2015 – 2017, (b) the OMI-Regional NO<sub>2</sub> product with only the air mass factor adjustment averaged over the same timeframe, and (c) the ratio between the two products. (d) Same as the top left plot, (e) the OMI-Regional NO<sub>2</sub> product with the air mass factor adjustment and spatial kernel averaged over the same timeframe, and (f) the ratio between the two products.

10

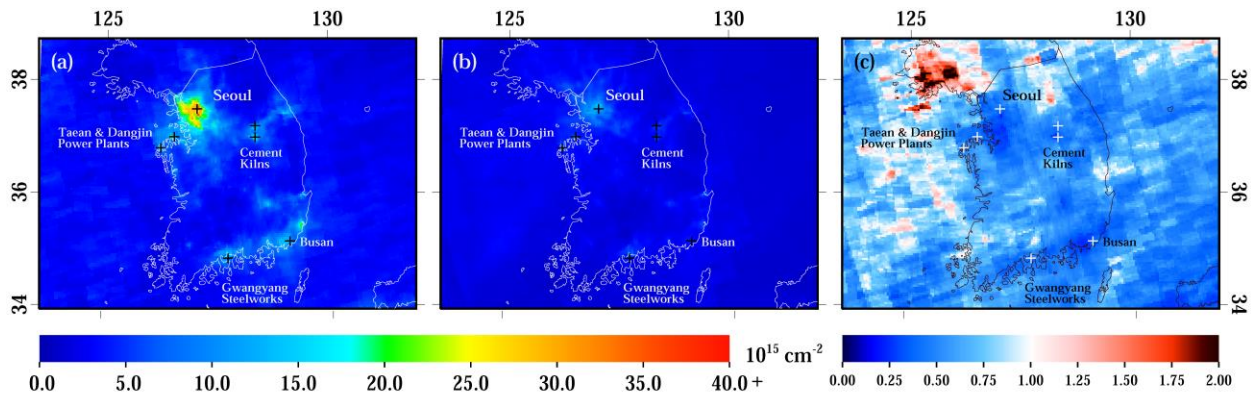


**Figure 3.** (a) The OMI-Regional  $\text{NO}_2$  product with the air mass factor adjustment and spatial kernel averaged during the month of May 2016, (b) the WRF-Chem model simulation showing only days with valid OMI measurements, and (c) the ratio between the two products. On average, there are only 9 valid OMI pixels per month observed at any given location on the Korean peninsula during May 2016.

5

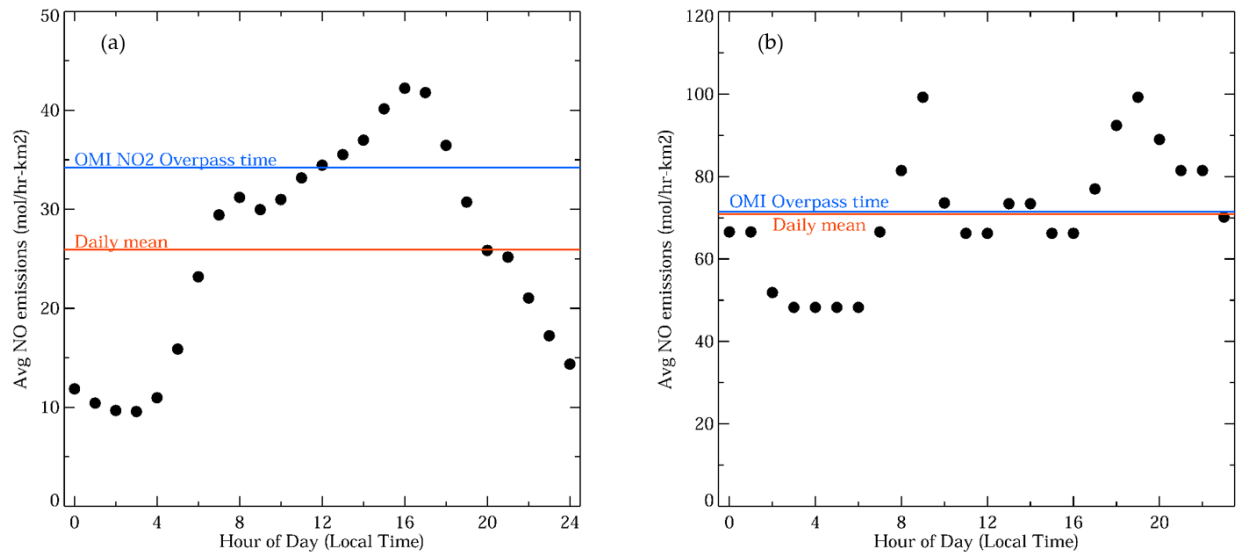


**Figure 4.** The diurnal profile of  $\text{NO}_x$  emission rates processed from the bottom-up inventory. (a) The diurnal profile of  $\text{NO}_x$  emission rates during a weekday in the eastern USA during July 2011 using SMOKE as the emissions pre-processor (Goldberg et al., 2016). (b) The diurnal profile of emission rates during a weekday in Korea during May 2016 using EPRES as the emissions pre-processor. Emission profiles in the right panel were used in the WRF-Chem simulation.

10

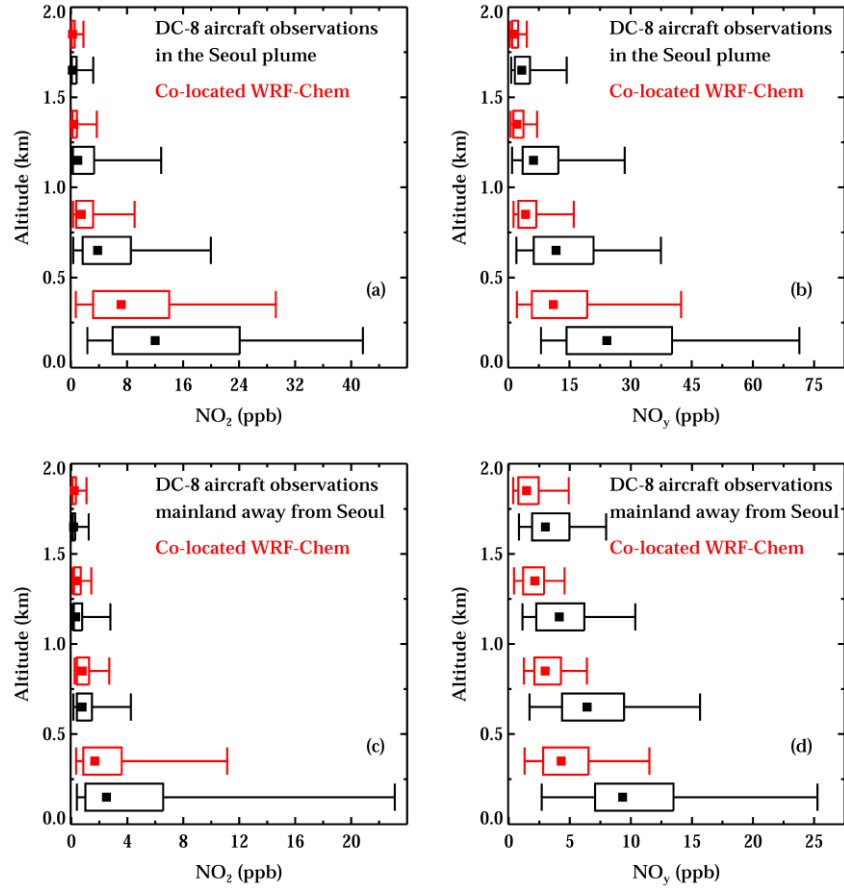
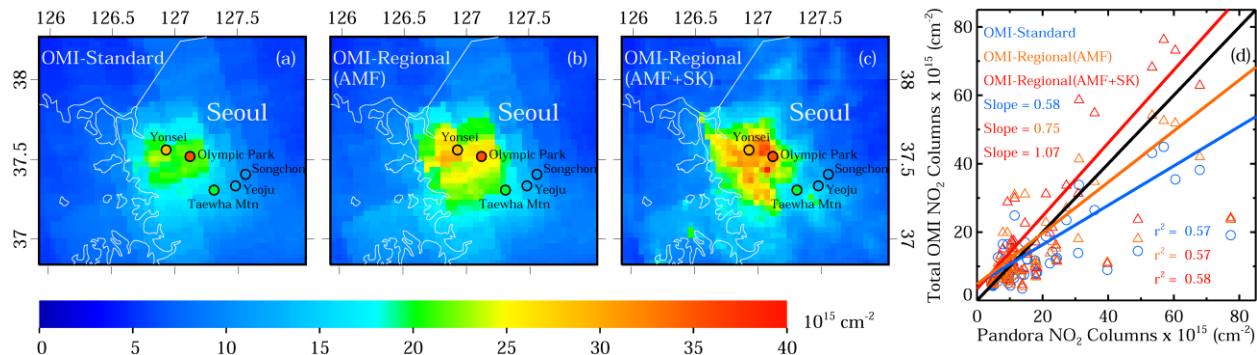


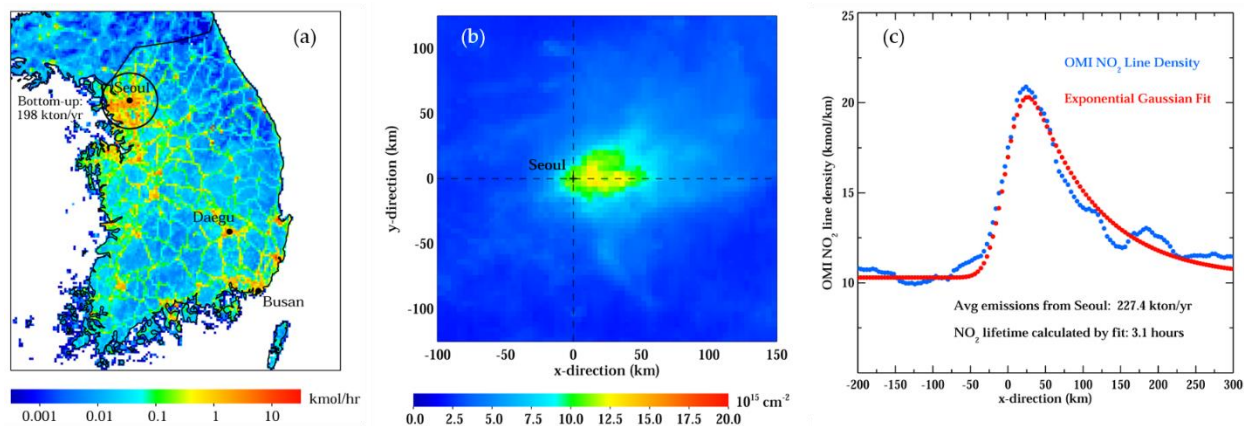
**Figure 5.** Measurements from the DC-8 aircraft binned by altitude in black. Co-located WRF-Chem within the same altitude bin as the aircraft observations are plotted above in red. Square dots represent the median values. Boxes represent the 25<sup>th</sup> and 75<sup>th</sup> percentiles, while whiskers represent the 5<sup>th</sup> and 95<sup>th</sup> percentiles. (a) Comparison of NO<sub>2</sub> in the Seoul plume (SW corner: 37.1° N, 127.05° E, NE corner: 37.75° N, 127.85° E) and (b) comparison of NO<sub>y</sub> in the Seoul plume, (c) comparison of NO<sub>2</sub> along in the “mainland transect” flights in the more rural areas outside of the Seoul metropolitan area on the Korean peninsula (SW corner: 34.0° N, 126.4° E, NE corner: 37.1° N, 130.0° E), and (d) comparison of NO<sub>y</sub> in areas outside of the Seoul metropolitan area on the Korean peninsula.

5

10

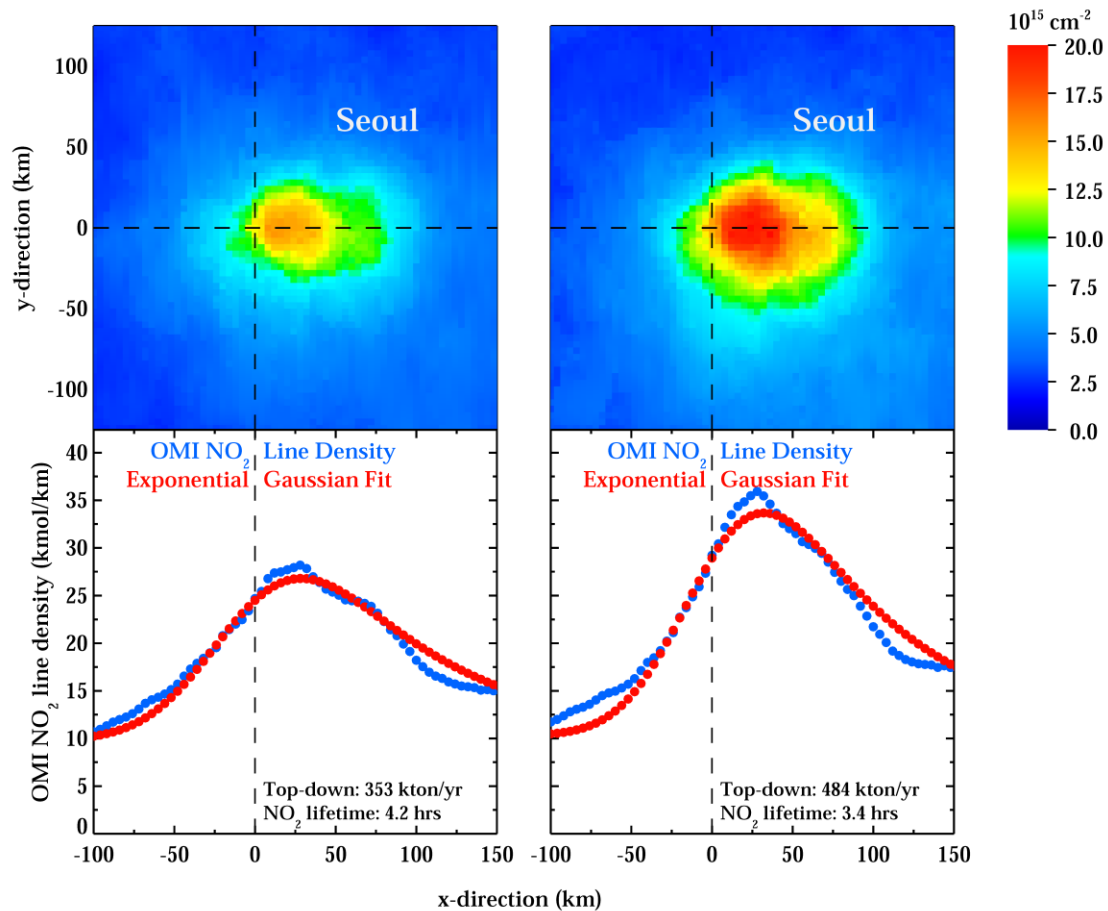


5 **Figure 6.** (a) Total vertical column contents from the OMI-Standard NO<sub>2</sub> product for May 2016, (b) same quantities from the OMI-Regional product with only the air mass factor adjustment (AMF) during the same timeframe, (c) center right same quantities from the OMI-Regional product with the air mass factor adjustment and spatial kernel (AMF+SK) during the same timeframe, and (d) a comparison between observed total column contents from the three OMI NO<sub>2</sub> products and Pandora NO<sub>2</sub> during May 2016. An average of Pandora 2-hour means co-located to valid daily OMI overpasses are overlaid in the spatial plots.



10 **Figure 7.** (a) Bottom-up NO<sub>x</sub> emissions inventory compiled for the KORUS-AQ field campaign, (b) the oversampled NO<sub>2</sub> plume rotated based on wind direction for Seoul, Korea from WRF-Chem (4 × 4 km<sup>2</sup>) for May 2016, and (c) NO<sub>2</sub> line densities integrating over the 240 km across plume width (-120 km to 120 km along the y-axis) and the corresponding EMG fit. NO<sub>x</sub> emission estimates are shown in units of kton/yr NO<sub>2</sub> equivalent and represent the mid-afternoon emissions rate.

15



5 **Figure 8.** Top panels represent the oversampled ( $4 \times 4 \text{ km}^2$ ) OMI NO<sub>2</sub> plume from Seoul rotated based on wind direction over a 9-month period, Apr – Jun 2015 – 2017, centered on May 2016. Bottom panels represent the OMI NO<sub>2</sub> line densities integrating over the 240 km across plume width (-120 km to 120 km along the y-axis of the top panels) and the corresponding EMG fit. Left panels are from the OMI-Standard NO<sub>2</sub> product and right panels are from the OMI-Regional NO<sub>2</sub> product. NO<sub>x</sub> emission estimates are shown in units of kton/yr NO<sub>2</sub> equivalent and represent the mid-afternoon emissions rate.

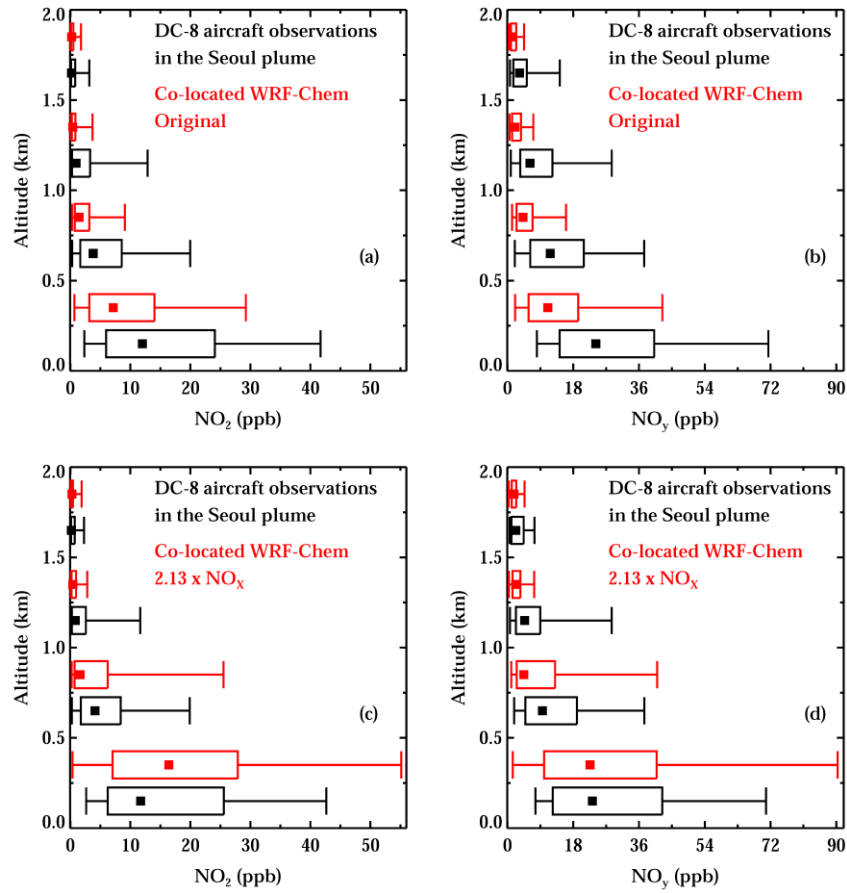


**Figure 9.** Measurements from the DC-8 aircraft binned by altitude in black. Co-located WRF-Chem within the same altitude bin as the aircraft observations are plotted above in red. Square dots represent the median values. Boxes represent the 25<sup>th</sup> and 75<sup>th</sup> percentiles, while whiskers represent the 5<sup>th</sup> and 95<sup>th</sup> percentiles. (a) Comparison of NO<sub>2</sub> in the Seoul plume (SW corner: 37.1° N, 127.05° E, NE corner: 37.75° N, 127.85° E) (b) comparison of NO<sub>y</sub> in the Seoul plume, (c) same as (a), but now using the WRF-Chem simulation with NO<sub>x</sub> emissions increased by a factor of 2.13 (d) same as (b), but now using the WRF-Chem simulation with NO<sub>x</sub> emissions increased by a factor of 2.13. Comparison in the Seoul plume for May 17, 2016 and May 18, 2016 between aircraft measurements and a 2 × NO<sub>x</sub> WRF-Chem simulation. DC-8 Aircraft measurements are binned by altitude in black. Co-located WRF-Chem within the same altitude bin as the aircraft observations are plotted above in red. Square dots represent the median values.

5

10

15

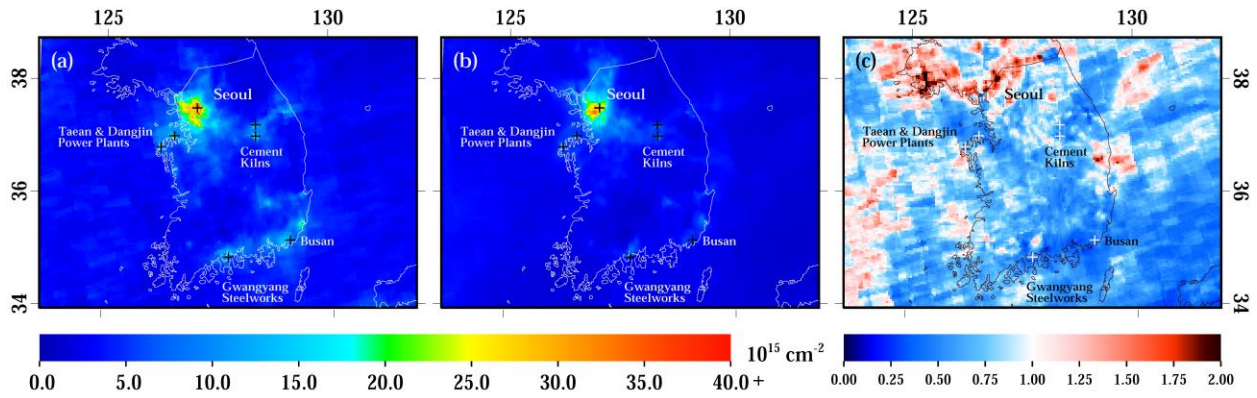


**Figure 10.** Same as Figure 3, but now showing the WRF-Chem simulation with  $\text{NO}_x$  emissions in the Seoul metropolitan area increased by a factor of 2.13 in panel (b).

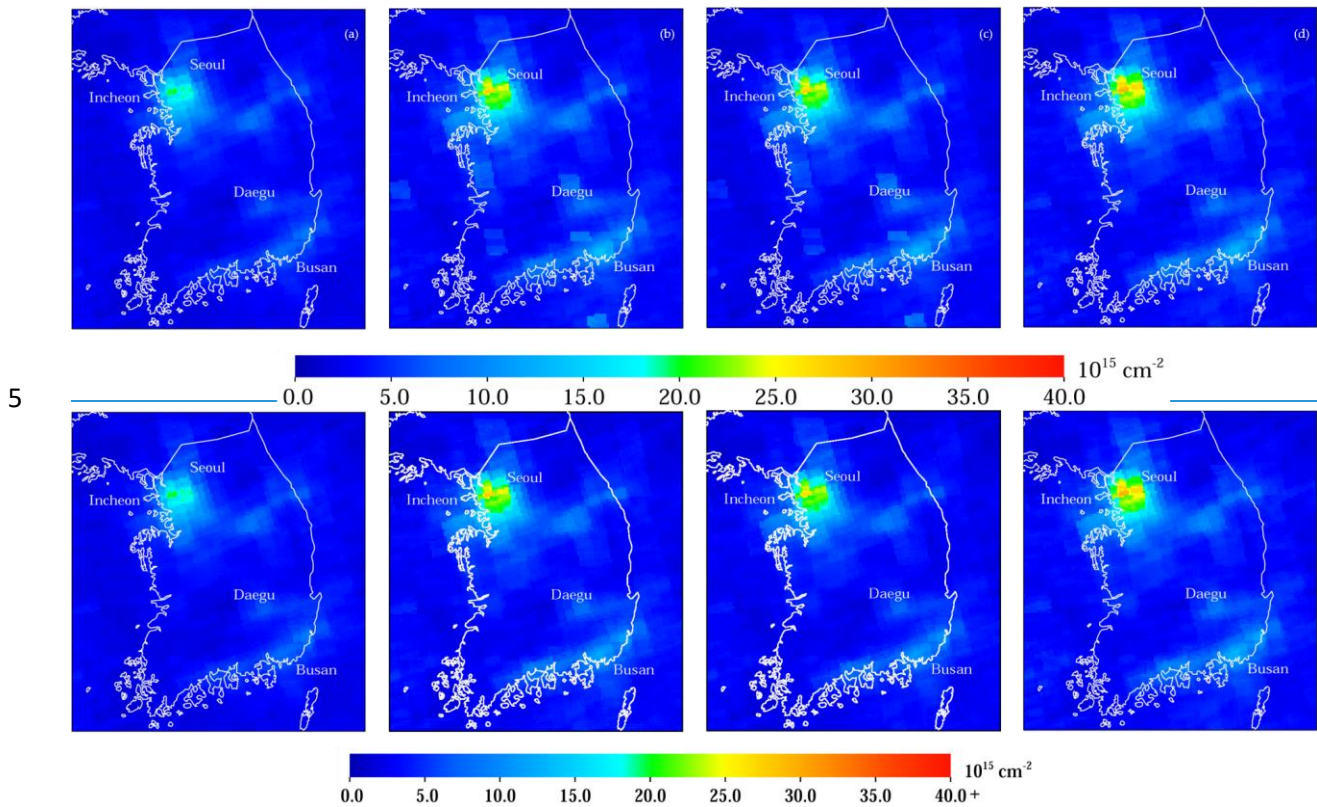


**Figure 11.** (a) The OMI-Standard product during the month of May 2016, (b) the OMI-Regional  $\text{NO}_2$  product with the WRF-Chem air mass factor adjustment and spatial kernel during the same period, (c) same as (b) but using WRF-Chem  $\text{NO}_2$  profiles scaled based on the aircraft comparison, and (d) same as (b) but using the WRF-Chem simulation with  $\text{NO}_x$  in the Seoul metropolitan area emissions increased by a factor of 2.13.